ASTROBIOLOGY
Volume 13, Number 3, 2013

DOI: 10.1089/ast.2012.0851

Tidal Venuses: Triggering a Climate Catastrophe via Tidal Heating

Rory Barnes,[1,2] Kristina Mullins,[1,2] Colin Goldblatt,[1,2,3] Victoria S. Meadows,[1,2] James F. Kasting,[2,4] and René Heller[5]

Abstract

Traditionally, stellar radiation has been the only heat source considered capable of determining global climate on long timescales. Here, we show that terrestrial exoplanets orbiting low-mass stars may be tidally heated at high-enough levels to induce a runaway greenhouse for a long-enough duration for all the hydrogen to escape. Without hydrogen, the planet no longer has water and cannot support life. We call these planets "Tidal Venuses" and the phenomenon a "tidal greenhouse." Tidal effects also circularize the orbit, which decreases tidal heating. Hence, some planets may form with large eccentricity, with its accompanying large tidal heating, and lose their water, but eventually settle into nearly circular orbits (*i.e.*, with negligible tidal heating) in the habitable zone (HZ). However, these planets are not habitable, as past tidal heating desiccated them, and hence should not be ranked highly for detailed follow-up observations aimed at detecting biosignatures. We simulated the evolution of hypothetical planetary systems in a quasi-continuous parameter distribution and found that we could constrain the history of the system by statistical arguments. Planets orbiting stars with masses $< 0.3\ M_{\rm Sun}$ may be in danger of desiccation via tidal heating. We have applied these concepts to Gl 667C c, a $\sim 4.5\ M_{\rm Earth}$ planet orbiting a $0.3\ M_{\rm Sun}$ star at 0.12 AU. We found that it probably did not lose its water via tidal heating, as orbital stability is unlikely for the high eccentricities required for the tidal greenhouse. As the inner edge of the HZ is defined by the onset of a runaway or moist greenhouse powered by radiation, our results represent a fundamental revision to the HZ for noncircular orbits. In the appendices we review (a) the moist and runaway greenhouses, (b) hydrogen escape, (c) stellar mass-radius and mass-luminosity relations, (d) terrestrial planet mass-radius relations, and (e) linear tidal theories. Key Words: Extrasolar terrestrial planets—Habitability—Habitable zone—Liquid water—Tides. Astrobiology 13, 225–250.

1. Introduction

All life on Earth requires liquid water. Not surprisingly, our search for life on exoplanets therefore begins with identifying environments that support it (Hart, 1979; Kasting *et al.*, 1993; Selsis *et al.*, 2007; von Bloh *et al.*, 2007). Many other features of a planet are also important, such as the mix of gases in the atmosphere and the interior's structure and energy budget, but current research has focused primarily on the stability of surface water. On Earth, liquid water persists primarily because the Sun's radiation heats the surface to a temperature between water's freezing and boiling points. Thus, the concept of a "habitable zone" (HZ) emerged, which is the region around a star in which insolation can maintain liquid water on the surface, assuming an Earth-like planet.

Stars have a wide range of luminosities, most of which are considerably lower than that of the Sun, yielding HZs that are closer in. At the extreme, the luminosity becomes so low that a planet orbiting at the stellar surface would be too cold to support liquid water on its surface. Such a star has no HZ. The recently discovered Y dwarf (which is not a star) WISEP J1828+2650 (Cushing *et al.*, 2011), with an effective temperature below 300 K, is an example of such a primary. For warmer stars, HZs may still be close enough in that nonradiative processes may impact habitability, such as stellar flaring (*e.g.*, Khodachenko *et al.*, 2007; Lammer *et al.*, 2007, 2010; Tian, 2009; Segura *et al.*, 2010), decreased initial volatile inventory (Lissauer, 2007; Raymond *et al.*, 2007), or tidal effects (*e.g.*, Kasting *et al.*, 1993; Joshi *et al.*, 1997; Correia *et al.*, 2008; Jackson *et al.*, 2008a; Barnes *et al.*, 2009a; Heller *et al.*,

[1]Astronomy Department, University of Washington, Seattle, Washington, USA.
[2]NASA Astrobiology Institute–Virtual Planetary Laboratory Lead Team, USA.
[3]Department of Earth and Ocean Science, University of Victoria, Victoria, Canada.
[4]Department of Geosciences, The Pennsylvania State University, State College, Pennsylvania, USA.
[5]Leibniz Institute for Astrophysics Potsdam (AIP), Potsdam, Germany.

2011). As the HZ of our Sun is too distant for these phenomena to affect Earth, we can currently only explore their role theoretically; consequently, many scientists consider close-in planets less favorable candidates for habitability.

Nevertheless, the last few years have seen renewed interest in the potential habitability of planets in orbit about low-luminosity objects (Scalo *et al.,* 2007; Tarter *et al.,* 2007; Lunine *et al.,* 2008; Monteiro, 2010; Agol, 2011; Bolmont *et al.,* 2011). This shift occurred because Earth-sized planets are easiest to detect around low-luminosity hosts, due to the larger mass and radius of the planet relative to the star. Furthermore, these objects are the most abundant in the solar neighborhood. Planets with masses between 1 and 10 $M_{\rm Earth}$, "super-Earths," have indeed been detected in the last few years around low-mass stars, such as Gl 581 d and Gl 667C c by radial velocity (Udry *et al.,* 2007; Mayor *et al.,* 2009; Vogt *et al.,* 2010; Bonfils *et al.,* 2011; Forveille *et al.,* 2011; Anglada-Escudé *et al.,* 2012; Delfosse *et al.,* 2012) and GJ 1214 b by transit (Charbonneau *et al.,* 2009; Sada *et al.,* 2010; Carter *et al.,* 2011; Kundurthy *et al.,* 2011). Several observational campaigns designed specifically to detect planets around low-mass stars are now underway (Nutzman and Charbonneau, 2008; Boss *et al.,* 2009; Zechmeister *et al.,* 2009; Bean *et al.,* 2010; Rodler *et al.,* 2011).

The inner edge of the HZ is especially prone to nonradiative phenomena. Traditionally, the inner boundary is defined by the stellar distance at which insolation is strong enough to remove all water in the atmosphere and on the surface (Kasting, 1988). Two different dehydrating scenarios (the "moist" and "runaway" greenhouse) are discussed in detail in Section 2 and Appendix A. Both require water vapor to penetrate a stratosphere, be dissociated (photolyzed) by high-energy radiation, and culminate in the escape of hydrogen. We call any process that can ultimately lead to total water loss a "desiccating greenhouse." Without sufficient hydrogen, water cannot form, and the planet will remain uninhabitable forever, unless a major, unlikely event occurs, for example, an impact by a water-rich body that simultaneously delivers water and changes the atmosphere in a way that halts the desiccating greenhouse. This definition of the inner edge is conservative because no known process can maintain habitability against a desiccating greenhouse. Other processes could be equally deleterious for life, but clearly total desiccation will terminate habitability.

We will discuss four types of terrestrial planets in this study, classified by their water content. "Wet" planets are terrestrial exoplanets that have a water content similar to that of Earth. "Dry" exoplanets have far less, $\sim$3 cm deep if condensed and spread globally, but are habitable (see Abe *et al.,* 2011). "Desiccated" planets have lost all their water through a desiccating greenhouse. Finally, "water worlds," (Léger *et al.,* 2004; Raymond *et al.,* 2004) are planets with a much larger inventory of water than modern Earth, for example, a warm Europa. This investigation explores the transition of wet, dry, and water worlds into the desiccated state.

Dole (1964) was the first to point out that terrestrial planets in the HZ of low-luminosity stars can have their spin altered by tidal interaction. In particular, the danger of synchronous rotation, that is, one hemisphere always facing the star, was emphasized. Kasting *et al.* (1993) quantified this concept and found that planets orbiting within the HZ of stars less than two-thirds the mass of the Sun were in danger of synchronization. Although their analysis was limited to Earth-like planets on circular orbits, a general belief developed that those planets could not be habitable, as one half of the planet would freeze while the other would roast.

Synchronization is certainly an important consideration when assessing habitability, and many investigations have explored its role, but with mixed results. Atmospheric modeling initially suggested that circulation will transport energy to the unlit side, ameliorating the extreme temperature difference (Joshi *et al.,* 1997). Some subsequent modeling has confirmed that synchronous rotators are likely to have super-rotating atmospheres (Joshi, 2003; Edson *et al.,* 2011; Heng and Vogt, 2011; Showman and Polvani, 2011), while others have discounted it (Wordsworth *et al.,* 2011), and still others have suggested that such a state might be beneficial at the outer edge of the HZ (Pierrehumbert, 2011). Taken together, these investigations suggest that synchronized planets should not be dismissed uniformly as uninhabitable. Hence, synchronization is not as stringent a constraint as desiccation and therefore is not an HZ boundary.

For many years, confusion also existed regarding the term "tidal locking." Many investigators assumed it was synonymous with "synchronous rotation." If the orbits are noncircular, as for many exoplanets (Butler *et al.,* 2006), then tidally evolved planets may reach an equilibrium state where they rotate faster than synchronous with an "equilibrium" or "pseudo-synchronous" period. This aspect of tidal theory has been known for decades (*e.g.,* Goldreich, 1966; Greenberg and Weidenschilling, 1984) but has only recently been pointed out for the case of exoplanets (Barnes *et al.,* 2008; Correia *et al.,* 2008; Ferraz-Mello *et al.,* 2008). Therefore, some exoplanets, such as Gl 581 d with an eccentricity of 0.38 (Mayor *et al.,* 2009), may be "tidally locked" but rotate about twice per orbit (Barnes *et al.,* 2008; Heller *et al.,* 2011). For more on this point, see the work of Murray and Dermott (1999), Chapter 5.2; and for a counterargument, see the work of Makarov and Efroimsky (2012). In the present paper, we use "tidally locked" to mean a planet rotating at the equilibrium period as determined by its eccentricity and obliquity; see Eqs. E7, E15–E16. In summary, a synchronously rotating planet is tidally locked (yet it could still have nonzero eccentricity and obliquity), but a tidally locked planet is not necessarily rotating synchronously.

Even if an orbit is currently circular, tides may not have driven the rotation to synchronous. If the orbit began with large eccentricity, tides will tend to damp it to zero, and we may expect it to be rotating synchronously. However, the planet could pass through one or more "spin-orbit resonances," where the planet's rotational frequency is commensurate with its orbital frequency (see, *e.g.,* Rodríguez *et al.,* 2012). For example, Mercury rotates three times for every two times it orbits the Sun, a 3:2 spin-orbit resonance. Spin-orbit resonances require a radially asymmetric mass distribution, which is likely for tidally deformed exoplanets but cannot be measured for the foreseeable future. A planet caught in a spin-orbit resonance may remain in that state even if circularized, as a resonance is a strong dynamical process. For any particular exoplanet, capture and retention into a spin-orbit resonance will be very difficult to constrain observationally, so all reasonable options should be considered. Therefore, synchronous rotation is unlikely for planets

with large eccentricities (Mercury's is 0.2) and not even guaranteed for a circular orbit. For more on spin-orbit resonances, the reader is referred to the work of Murray and Dermott (1999), Chapter 5.4.

As tidal locking of the planetary rotation is not an absolute constraint on habitability, we turn to tidal heating as the other tidal phenomenon most likely to affect planetary habitability. As a planet moves from periastron, its closest approach to the star, to apoastron, the farthest point, and back again, the gravitational force changes, being inversely proportional to distance squared. This difference creates an oscillating strain on the planet that causes its shape to vary periodically. The rigidity of the planet resists the changes in shape, and friction generates heat. This energy production is called tidal heating.

Tidal heating is responsible for the volcanism on Io (Strom *et al.,* 1979; Laver *et al.,* 2007), which was predicted by Peale *et al.* (1979) with the use of tidal theory. Io is a small body orbiting Jupiter with an eccentricity of 0.0041 that is maintained by the gravitational perturbations of its fellow Galilean moons and shows global volcanism that resurfaces the planet on a timescale of 100 to 10^5 years (Johnson *et al.,* 1979; Blaney *et al.,* 1995; McEwen *et al.,* 2004). The masses of Jupiter and Io are orders of magnitude smaller than a star and terrestrial exoplanet; thus the latter have a much larger reservoir of orbital and rotational energy available for tidal heating. Moreover, some exoplanets have been found with orbital eccentricities larger than 0.9 (Naef *et al.,* 2001; Jones *et al.,* 2006; Tamuz *et al.,* 2008). Thus, the tidal heating of terrestrial exoplanets may be much more effective than that which occurs on Io (Jackson *et al.,* 2008a, 2008c; Barnes *et al.,* 2009a, 2010; Heller *et al.,* 2011). This expectation led to the proposition that terrestrial exoplanets with surface heat fluxes as large or larger than Io's should be classified as "Super-Ios" rather than "Super-Earths" (Barnes *et al.,* 2009b). Numerous Super-Io candidates exist, such as CoRoT-7 b (Léger *et al.,* 2009; Barnes *et al.,* 2010), Gl 581 e (Mayor *et al.,* 2009), 55 Cnc e (McArthur *et al.,* 2004; Dawson and Fabrycky, 2010; Winn *et al.,* 2011), and Kepler-10 b (Batalha *et al.,* 2011), but none is in the HZ.

Jackson *et al.* (2008a) and Barnes *et al.* (2009a) considered Io's heat flux, ~ 2 W m^{-2} (Veeder *et al.,* 1994; Spencer *et al.,* 2000; McEwen *et al.,* 2004), to be an upper limit for habitability, arguing that Io-like surfaces are dangerous for habitability. However, 2 W m^{-2} may not be sufficient to sterilize a planet and so should not be considered a hard limit to habitability. For example, the heat flow in inhabited hydrothermal vent systems on Earth, such as the Endeavour segment of the Juan de Fuca Ridge (Holden *et al.,* 1998), is ~ 30 W m^{-2} (Fontaine *et al.,* 2011). Thus, a water world with tens of watts per square meter of energy output could support life. While Io-like volcanism is clearly an issue for habitability, it may not always lead to sterilization. However, if the tidal heating can maintain a desiccating greenhouse long enough for all the water to be lost, then the planet becomes uninhabitable and is highly unlikely to ever regain habitability.

Calculations of the inner edge of the HZ have traditionally assumed the primary energy source at the surface is stellar radiation, as is the case for Earth. Following Barnes *et al.* (2009a), we call that type of HZ an "insolation habitable zone" (IHZ), as starlight is the only energy source considered. In this investigation, we identify the amount of tidal heating that triggers a desiccating greenhouse, as well as the combinations of physical and orbital parameters for which tidal heating could yield it. We find such a state is predicted by current models and dub such a world a "Tidal Venus" and the phenomenon that produces it a "tidal greenhouse." The tidal greenhouse would probably have the same effect on habitability as one caused by irradiation and hence should be considered as hard a limit to habitability as a traditional, insolation-driven desiccating greenhouse.

In this study, we define the limits of Tidal Venuses in terms of stellar and planetary mass, M_* and M_p, respectively, the orbital semimajor axis a, orbital eccentricity e, planetary radius R_p, planetary obliquity ψ_p, and planetary spin frequency ω_p. Some of these quantities are easily observed by current technology; others require special geometries and the next generation of space telescopes. Therefore, for the next decade, not all newly found planets in an IHZ will have well-constrained tidal heating. This study provides a framework for identifying the range of tidal heating on terrestrial planets orbiting in the IHZ of low-luminosity stars. As can be seen below, the story is complicated and involves a large parameter space, but is tractable.

We first review the surface conditions that lead to a greenhouse state in Section 2, including an extended discussion of the moist and runaway greenhouses (Appendix A); a short review of hydrogen escape driven by high-energy radiation (Appendix B); the relationships between mass, radius, and luminosity for low-mass, hydrogen-burning stars, "M dwarfs," or "late-type stars" in the parlance of astrophysics; the extent of the IHZ (Appendix C); and mass-radius relationships for terrestrial exoplanets (Appendix D). We then briefly describe tidal heating in Section 3 with details in Appendix E. Next, we show that tidal heating alone can produce surface conditions capable of triggering a runaway greenhouse on planets orbiting M dwarfs (Section 4). Then we explore how past tidal heating may preclude habitability of planets found in the IHZ regardless of their current tidal heating (Section 5). In Section 6, we then consider the Gl 667C system, which contains two potentially habitable planets, and find that tidal heating is unlikely to have sterilized either. In Section 7, we discuss the results, and finally in Section 8 we draw our conclusions.

2. The Inner Edge of the Habitable Zone

Planets with surface water will always have water vapor in their atmospheres. The amount of water vapor present in equilibrium with a liquid surface is described by the saturation vapor pressure p_sat, which is the pressure exerted by water vapor in thermodynamic equilibrium with standing surface water. The value of p_sat depends exponentially on temperature: a warmer planet will have much more water vapor in its atmosphere. Water vapor is a greenhouse gas (see below), so a warmer planet will have a stronger greenhouse effect, which enhances warming, a positive (but not necessarily runaway) feedback.

Atmospheric gases on Earth—and those that we expect on habitable Earth-like planets—are mostly transparent to optical wavelengths, so starlight is able to heat the surface. The surface in turn heats the air in contact with it, which rises, expanding and cooling adiabatically. As the air cools, water

vapor condenses, releasing latent heat and so slowing the cooling. The net rate of temperature decrease with height is called the "moist adiabatic lapse rate," setting the mean temperature–pressure (T–p) structure of Earth's troposphere (the lower region of the atmosphere affected by convection and bounded at the bottom and top by the planetary surface and the tropopause, the altitude at which temperature stops dropping with height).

Atmospheric gases that absorb radiation at similar wavelengths to the radiative emission of the planet (thermal IR for Earth and any habitable planet) are termed "greenhouse gases"; these cause a "greenhouse effect." The most important greenhouse gases for Earth are water vapor and carbon dioxide. They absorb radiation emitted by the surface and then reemit, both downward toward the surface and upward into space. Energy radiated toward the surface (commonly called back radiation) heats the surface. Most importantly, as the atmosphere is cooler than the surface, the amount of radiation emitted to space from the atmosphere is less than the amount of energy emitted by the surface. Thus, the presence of a greenhouse atmosphere means the surface temperature is warmer than the equilibrium temperature of the planet.

Earth's greenhouse effect keeps the planet warm enough to be habitable; without it Earth's surface would be at the planet's equilibrium temperature, a barren 255 K. However, stronger and more water-vapor-rich greenhouse atmospheres can render the planet uninhabitable through high-temperature sterilization and/or desiccation (loss of the ocean), and thus define the inner edge of the HZ. There are two physically distinct situations that lead to loss of habitability, the "runaway greenhouse" and "moist greenhouse."

The runaway greenhouse was recently reviewed by Goldblatt and Watson (2012), so we provide a summary description only. As the planet warms, the amount of water vapor in the atmosphere increases such that water becomes a major constituent of the atmosphere and ultimately the dominant one. Consequently, the moist adiabatic lapse rate tends toward the saturation vapor pressure curve for water, and the T–p structure of the atmosphere becomes fixed. Concurrently, the atmosphere becomes optically thick in the thermal IR, such that only the upper troposphere can emit to space. As the T–p structure is fixed, the emitted radiation is also fixed, imposing a limit on the outgoing radiation ($F_{\rm crit}$) from the troposphere. Values for $F_{\rm crit}$ from the literature are typically 285 W m^{-2} to 310 W m^{-2} for a 1 $M_{\rm Earth}$ planet (Pollack, 1971; Watson *et al.,* 1984; Abe and Matsui, 1988; Kasting, 1988; Pierrehumbert, 2010). The physics of this limit were described in more detail by Simpson (1927) and Nakajima *et al.* (1992). [Komabayashi (1967) and Ingersoll (1969) described a stratospheric limit at a higher flux, 385 W m^{-2}, which is never reached in practice.] If the amount of energy supplied to the atmosphere by the Sun (Simpson, 1927), impacts (Abe and Matsui, 1988), or tidal heating (this work) were to exceed $F_{\rm crit}$, then the atmosphere would not be able to maintain radiation balance, and runaway heating of the surface would ensue, causing evaporation of the entire ocean. Radiation balance would be regained either (a) when the surface temperature reaches $\sim$1400 K, at which point enough radiation is emitted in the near-IR where water vapor is not a good absorber or (b) if all the water vapor is lost from the atmosphere.

One likely water loss mechanism is hydrogen escape to space. Today, little water vapor reaches the upper atmosphere because the tropopause acts as a "cold trap"; almost all water has condensed lower in the atmosphere, so the tropopause water vapor mixing ratio (the abundance of water vapor in the atmosphere, expressed as the ratio of the mass of water vapor to the mass of dry air) is low. Water vapor transport above here is generally diffusive, leading to a constant water vapor mixing ratio in the upper atmosphere. (More precisely, in Earth's atmosphere, water vapor increases with altitude in the stratosphere due to methane oxidation and decreases with altitude in the next higher atmospheric layer, the mesosphere, due to photolysis; however, the total hydrogen mixing ratio is conserved, and the hydrogen escape rate depends on this value.) Thus, water is not a strong source of escaping hydrogen, and the overall escape rate is low. However, in the runaway greenhouse the atmosphere becomes predominantly water, so no such constraint applies, and hydrogen may escape hydrodynamically to space (Kasting and Pollack, 1983). The rate will depend on the amount of extreme ultraviolet (XUV, 1–1200 Å) radiation absorbed in the highest part of the atmosphere, so this process is also limited by the available stellar XUV energy (Watson *et al.,* 1981). A Venus-sized planet at the inner edge of the HZ could lose an ocean the size of Earth's in $\sim 10^8$ years (Watson *et al.,* 1981); we refer to this as the desiccation time, $t_{\rm des}$ (discussed further below). Deuterium would be retained preferentially over ordinary hydrogen during hydrogen escape. Enrichment of D/H on Venus implies that Venus lost a substantial amount of water to space (Donahue *et al.,* 1982; de Bergh, 1993), likely after experiencing a runaway greenhouse.

We adopt $t_{\rm des} = 10^8$ years based on the work on Venus as well as on calculations presented in Appendix B for a terrestrial planet orbiting a very low-mass star. Such stars are very active and emit strongly in the near UV, especially when they are young (*e.g.,* West *et al.,* 2008), but the total flux is still less than that of the present-day Sun (Fleming *et al.,* 1993), and the XUV flux (which drives hydrodynamic escape) is not well known. Thus, we expect a range of $t_{\rm des}$ to exist, especially since the orbit evolves with time due to tides, but choose this value for simplicity. The model described in Appendix B can be applied to individual cases when observations permit realistic modeling. We stress that there are many unknowns that may affect the actual value of $t_{\rm des}$. The masses of exoplanet oceans are unknown. Earth's mantle contains a few ocean masses of water (Bell and Rossman, 1992; Murakami *et al.,* 2002; Marty and Yokochim, 2006), so it is possible that the surface of a planet could acquire a new ocean via outgassing after desiccation and become habitable again. Thus, we cannot conclude with certainty that a planet with a desiccated atmosphere will never be habitable in the future. However, we also expect rapid mantle overturn during strong tidal heating; hence the entire water inventory may actually be lost. We therefore assume that the tidal greenhouse is highly likely to sterilize a planet permanently.

The moist greenhouse (Kasting, 1988) describes a warm atmosphere, in which the whole troposphere is assumed to be water vapor–saturated and is underlain by a liquid ocean. As the surface temperature increases, the tropopause is pushed higher (to lower pressure), given the reasonable assumption of a constant tropopause temperature. While the

saturation vapor pressure at the tropopause is, by this assumption, constant, the saturation mixing ratio of water at the tropopause (p_{sat}/p_{trop}) increases as the tropopause moves higher, where p_{trop} is the atmospheric pressure at the tropopause. The cold trap is then no longer effective, substantial water vapor penetrates the stratosphere, and water-derived hydrogen escape can be effective. The planet may thus gradually desiccate while in a hot, but stable, climate. This process could be driven by high greenhouse gas inventories rather than external heating.

A key distinction between the runaway and moist greenhouses is that the former happens when a known flux of energy is supplied to the planet, whereas the latter depends most strongly on surface temperature. The runaway greenhouse occurs because water vapor is a greenhouse gas and can therefore trap heat near the surface: hence it is only a function of the absorptive properties of water and the energy flux. The moist greenhouse occurs when the temperature at the tropopause is large enough that water does not condense and is therefore able to escape to the stratosphere where it can be photolyzed. Increasing the planet's inventory of noncondensible greenhouse gases has a small effect on the runaway greenhouse limit but can drive the moist greenhouse since the relative amount of H_2O is lower. Thus, the runaway greenhouse is a more conservative choice to demarcate the inner edge of the IHZ in the sense that it depends solely on water, whereas knowledge of the atmospheric composition may not be available to assess the likelihood of a moist greenhouse.

In Fig. 1, we show the moist and runaway greenhouse for wet planets in orbit around M dwarfs. See Appendices A, C, and D for a discussion of IHZ limits, stellar mass-radius and mass-luminosity relationships, and terrestrial mass-radius relationships. In Fig. 1, the gray regions are the limits of the moist greenhouse as presented in Selsis *et al.* (2007). At the inner edge, Selsis *et al.* (2007) found that 300 W m^{-2} triggers the moist greenhouse on a 1 M_{Earth} planet, and from left to right the limits assumed 100%, 50%, and 0% cloud cover (for a 0.25 M_{Sun} star these limits correspond to bond albedos of 0.75, 0.49, and 0.23, respectively). The solid curve is the runaway greenhouse limit (Pierrehumbert, 2010) for a 30 M_{Earth} planet and dashed for a 0.3 M_{Earth} planet, both with an albedo of 0.49 (compare to the medium gray). As expected (see Appendix A), the smaller planet's inner edge lies at larger semimajor axis than the 1 M_{Earth} moist greenhouse limit, which in turn lies farther out than the 30 M_{Earth} runaway greenhouse limit.

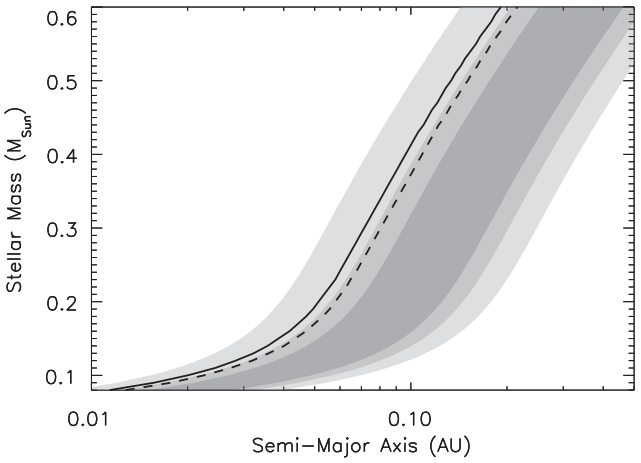

FIG. 1. Comparison of HZ boundaries for different planetary masses and desiccating greenhouses. The shaded regions represent the IHZ boundaries from Selsis *et al.* (2007): dark gray assumes no cloud coverage, medium gray 50%, and light gray 100%, and assuming a 1 M_{Earth} planet. The black curves represent the runaway greenhouse limit from Pierrehumbert (2011), with a planetary albedo of 0.49. The solid curve is for a 30 M_{Earth} planet, dashed for a 0.3 M_{Earth} planet. For these calculations we used the stellar mass-radius relationship from Bayless and Orosz (2006), the mass-luminosity relationship from Reid and Hawley (2000), and the terrestrial mass-radius relationship from Sotin *et al.* (2007).

We have presented the classical description of the desiccation at the inner edge of the HZ above. Various complications are worthy of note. Water on a dry planet will get trapped at the poles, which makes a moist or runaway greenhouse harder to achieve and means that the inner edge of the HZ is nearer the star (Abe *et al.*, 2011). We do not include that limit in Fig. 1, but we return to it in Section 4. Figure 1 assumes the planetary orbit is circular. However, for the many exoplanets with (highly) eccentric orbits (Butler *et al.*, 2006), the total irradiation over an orbit determines the annual-averaged surface temperature (Williams and Pollard, 2002) and pushes the IHZ boundaries out by a factor of $(1-e^2)^{-1/4}$ (Barnes *et al.*, 2008).

3. Tidal Heating

Tidal heating is responsible for the volcanic activity on Io (Peale *et al.*, 1979) and probably the geysers of Enceladus (Hansen *et al.*, 2006; Porco *et al.*, 2006; Hurford *et al.*, 2007). Tidal theory has a long and established body of work; however, tidal processes remain poorly understood. The difficulty lies in the complexity of the energy dissipation processes and the very long timescales associated with tidal evolution. The Earth-Moon system is the most accurately studied, with lunar laser ranging providing a precise measurement of the recession of the Moon due to tides of $\sim$38 mm/yr (Dickey *et al.*, 1994), as well as direct measurements of the locations of dissipation in the ocean (Egbert and Ray, 2000). However, using the currently estimated tidal dissipation parameters to extrapolate backward in time predicts that the Moon was at Earth's surface about $\sim$2 Gyr ago (MacDonald, 1964), which contradicts the standard impact model for the lunar origin [note that numerous issues remain such as the origin of Earth's and the Moon's obliquities (Touma and Wisdom, 1994) and the perturbations from other planets (Ćuk, 2007)]. The deceleration of Io's orbital velocity has also been tentatively detected and seems broadly consistent with tidal theory (Aksnes and Franklin, 2001; Lainey *et al.*, 2009). However, these data lie in the same regime, that of nearly circular orbits. Exoplanets have been found with extremely eccentric orbits, so we can only extrapolate from our Solar System cautiously. The details of tidal theory are complicated; hence we relegate the discussion to Appendix E.

Two end-member models of tidal theory have been applied to exoplanets and the bodies of our solar system: one assumes the energy dissipation gives a constant phase lag in

the periodic distortion (CPL), and the other assumes a constant time lag (CTL) (Greenberg, 2009). While simple and linear, such models are probably commensurate with the dearth of information we have about exoplanet interior processes. More complicated models have been constructed, and they reproduce the above models for certain choices of internal composition, structure, and energy transport (*e.g.,* Henning *et al.,* 2009). Thus, the CPL and CTL models can provide important and accurate insight into the tidal evolution of exoplanets.

These models converge at $e=0$ and have been shown to be nearly identical for $e \leq 0.2$ (Leconte *et al.,* 2010) and when using Eq. E21. However, for $e>0.3$, they diverge significantly. We urge caution when interpreting results in the upcoming sections, which allow e to be as large as 0.8. We include this range primarily for illustrative purposes and as a baseline for any future work that may include nonlinear effects.

The tidal heating of a body is provided in Eqs. E10 and E18 for the CPL and CTL models, respectively. Averaging the heating rate of the entire planetary surface gives the surface energy flux due to tides, $F_{\rm tide}$. In those equations, the strength of the tidal effects is parameterized as a "tidal quality factor" Q (CPL) or "tidal time lag" τ (CTL), which are notoriously difficult to measure or estimate from first principles. Earth's current values are $Q=12$ (Yoder, 1995) and $\tau=638$ s (Lambeck, 1977; Neron de Surgy and Laskar, 1997), respectively. However, as noted above, these values predict too short a lifetime of the Moon. This discrepancy has led to the notion that Earth's response to lunar tides has evolved with time, possibly due to changing size, shape, and seafloor topography of the oceans, affecting the ocean current's response to the tidal potential. Measurements of the dry bodies in our solar system have found that their Q values tend to cluster around 100; see Appendix E.

Recent satellite observations of Earth have revealed the locations of tidal dissipation in our oceans (Egbert and Ray, 2000). Tides force water through shallow seas and straits, which causes energy dissipation. In the open ocean, tidal dissipation is probably a nonlinear process in which currents are disrupted by seafloor topography. The presence of the ocean provides more opportunity for tidal dissipation than on dry planets, and we assume that most dissipation on habitable exoplanets will also occur in their oceans. Therefore, for the following calculations, we assume modern Earth-like planets with $Q=10$–100 or $\tau=64$–640 s.

4. Tidal Venuses

We computed tidal heating rates for a range of planetary, stellar, and orbital parameters and found that tidal heating can be strong enough on some planets to trigger a runaway greenhouse. In Fig. 2, we show the configurations that predict this state around four different hypothetical M dwarfs. The IHZ boundaries are the moist greenhouse limits of Selsis *et al.* (2007) and with the same format as Fig. 1. The colored curves mark where $F_{\rm tide}=F_{\rm crit}$. Red curves assume the CTL model, blue the CPL with discrete rotation states; see Appendix E.1. Solid curves assume the Pierrehumbert (2011) runaway greenhouse model, and dotted the dry world model of Abe *et al.* (2011); see Fig. A1 in Appendix A. For these latter worlds, we choose $Q=100$, as they do not have oceans. Thick lines are for a 10 $M_{\rm Earth}$ planet and thin for 1 $M_{\rm Earth}$ [Abe *et al.* (2011) only considered a 1 $M_{\rm Earth}$ planet]. Note that our choice for the relationship between Q and τ influences which model predicts more heating. If we had chosen the same relationship as that of Heller *et al.* (2011), we would have found that the CTL model predicts more heating than CPL; compare their Fig. 5.

For the lowest-mass M dwarfs, the HZ is significantly reduced due to tidal heating. For masses larger than 0.25 $M_{\rm Sun}$, a tidal greenhouse in the IHZ is only possible on large-mass planets with very large eccentricities. For lower mass stars, our model predicts a tidal greenhouse at low eccentricities where tidal theory is most likely valid. Figure 2 shows that a planet may have a climate catastrophe due to tide-driven overheating even if it is far enough from the star that stellar radiative heating alone would not preclude habitability.

The difference between curves representing equal-mass planets is due to the frequency dependence of the CTL model. For Earth, the frequency is the mean motion of the lunar orbit, but a planet at $a=0.035$ AU, that is, the middle of the HZ, orbits in about 1 week. One could formally adjust τ so that it is equivalent to a Q of 10 (see, *e.g.,* Matsumura *et al.,* 2010; Heller *et al.,* 2011; Eq. E21); then the curves would lie in a similar location. The unknown tidal response of terrestrial bodies and the absence of an unambiguous translation from the CPL to the CTL model motivates our choice of adopting present-Earth values for all planets at all frequencies.

Regions to the left of the colored curves in Fig. 2 can produce Tidal Venuses if the planets remain there longer than $t_{\rm des}$. In Fig. 3, we show the evolution of two example systems consisting of a 10 $M_{\rm Earth}$ planet orbiting a 0.1 $M_{\rm Sun}$ star, using both the CPL and CTL models. For the CPL case, the planet begins with semimajor axis $a=0.04$ AU, and $e=0.3$. The planet is assumed to be spin-locked and with zero obliquity. This orbit is toward the outer edge of the IHZ and with the typical eccentricity of known exoplanets. For the CTL case, everything is the same, except the initial a is 0.035 AU, as the Tidal Venus region lies closer to the star. The top panel in Fig. 3 shows the evolution of a, the next panels down show e, then insolation $F_{\rm insol}$, then tidal heat flux $F_{\rm tide}$, and finally the sum of the insolation and tidal heat flux, $F_{\rm total}$. The tidal heat flux generated in the planet in the CPL case has decreased to $F_{\rm crit}=345$ W m^{-2} at 200 Myr, and the sum of tidal heating and insolation reaches $F_{\rm crit}$ at 275 Myr. In the CTL case, $F_{\rm tide}=F_{\rm crit}$ at 130 Myr, and $F_{\rm total}=F_{\rm crit}$ at 275 Myr. We conclude that planets orbiting low-mass stars on eccentric orbits may experience tidal greenhouse conditions long enough to become uninhabitable.

The CPL model predicts a will increase through angular momentum transfer with the star, for which we assume a rotation period of 30 days, a tidal Q of 10^6, a radius determined by the Reid and Hawley (2000) relation, and both the radius of gyration and Love number of degree 2 are 0.5. However, this orbital expansion is a result of the discrete nature of the CPL model, which only includes four "tidal waves," see Appendix E.1. In Fig. 3, the planet initially spins three times per two orbits; hence $\varepsilon_{1,1}=0$, see Eq. E5, eliminating one of the terms in da/dt. Note that once the eccentricity drops below $\sqrt{1/19}$ the spin rate becomes synchronous (see Appendix E.3); then $\varepsilon_{0,1}=0$ but $\varepsilon_{1,1}=1$, and then $da/dt<0$. For this example, that transition occurs at 375 Myr and is not shown in Fig. 3. This point illustrates the complexity inherent in this commonly used tidal model.

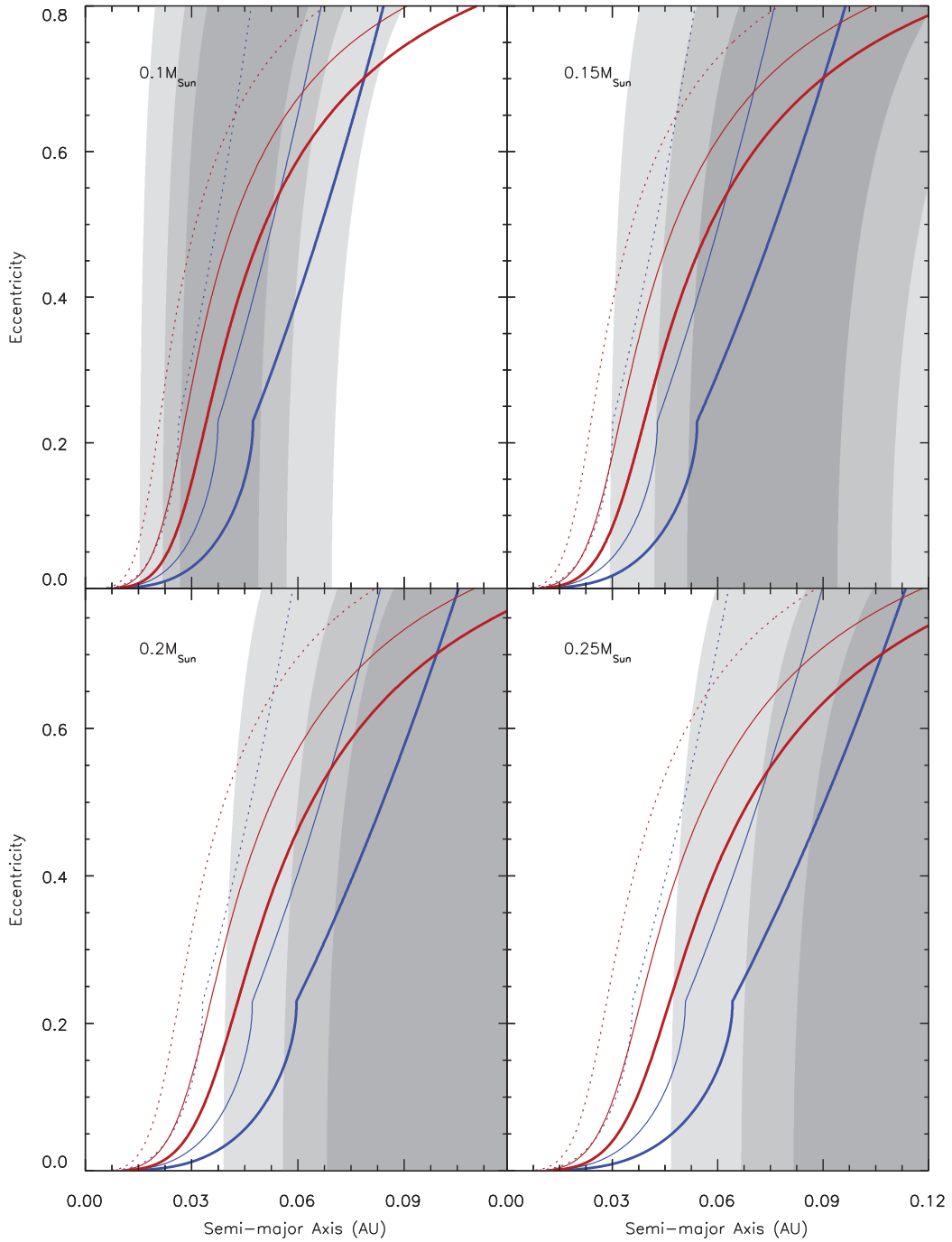

FIG. 2. Parameter space of the Tidal Venus. The top left panel is a 0.1 $M_{\rm Sun}$ star, top right 0.15 $M_{\rm Sun}$, bottom left 0.2 $M_{\rm Sun}$, and bottom right 0.25 $M_{\rm Sun}$. The grayscale represents the Selsis *et al.* (2007) IHZ boundaries: from lightest to darkest gray, the cloud coverage is 100%, 50%, and 0%, respectively. The colored curves mark where $F_{\rm tide} = F_{\rm crit}$. Red curves assume the CTL model, blue the CPL. Solid curves assume the Pierrehumbert (2011) runaway greenhouse model and dotted the dry world model of Abe *et al.* (2011). Thick lines are for a 10 $M_{\rm Earth}$ planet and thin for 1 $M_{\rm Earth}$. Tidal Venuses lie to the left of these curves.

5. Constraining Observed Planets

The previous section demonstrated that planets may become desiccated by tidal heating, but in many cases we will be more interested in the possibility that such a condition developed on a planet that we have discovered. As tides tend to circularize orbits, we may find a planet in the IHZ with low eccentricity that experienced a tidal greenhouse early on and is hence currently uninhabitable. In this section, we describe how to evaluate a known planet's probability for habitability based on past tidal heating.

To model the tidal heating history of an exoplanet, we require knowledge of $M_{\rm p}$, $R_{\rm p}$, a, e, M_*, R_*, and age. Exoplanets are predominantly discovered by radial velocity and

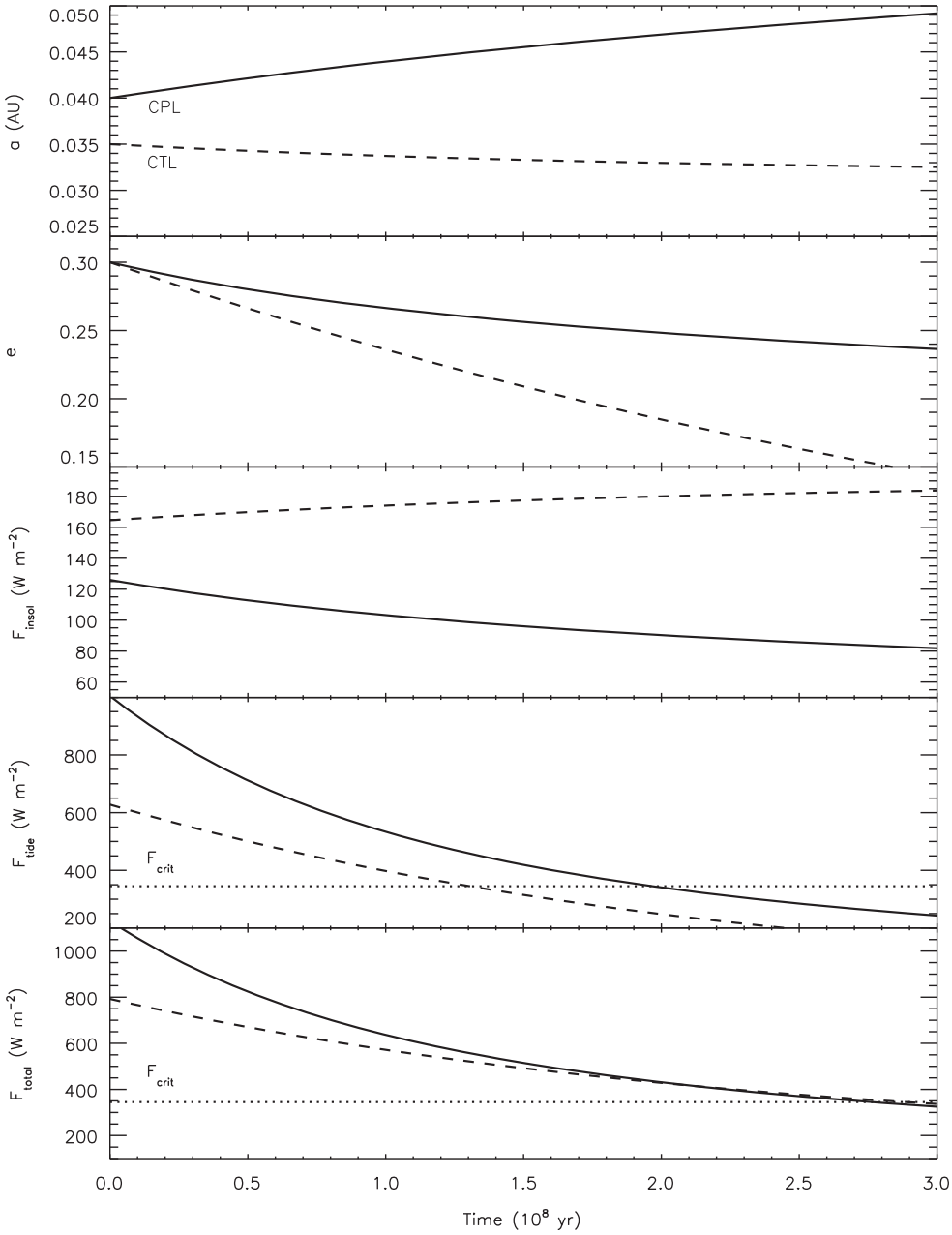

FIG. 3. Evolution of a 10 $M_{\rm Earth}$ planet orbiting a 0.1 $M_{\rm Sun}$ star with an initial orbit of $a = 0.04$ AU, $e = 0.3$. *Top:* semimajor axis evolution. *Top middle:* eccentricity evolution. *Middle:* insolation evolution. *Bottom middle:* tidal heat flux evolution. *Bottom:* total surface heat flux (insolation + tidal).

transit studies that can provide a and e, while the others can be modeled from the stellar spectrum. If some of these values are unknown, we can often use scaling relations to estimate them; see Appendices C–D. From this information, one can estimate the tidal heating history of a planet, using the tidal evolution equations (Appendix E), and hence estimate the probability that the planet has lost its water. As an example, consider the hypothetical situation in which a terrestrial-scale planet has been discovered in orbit about an M dwarf. Further, the planet lies near the inner edge of the IHZ and has a low eccentricity. To evaluate past tidal heating, we created four systems with different stellar and planetary properties, applied reasonable uncertainties to each observable property, chose non-observable properties via appropriate scaling laws, and modeled the system's history. In particular, we assume that the planet's mass lies between 1 and 5 $M_{\rm Earth}$, has an eccentricity less than 0.1, a tidal $Q_{\rm p}$ ($\tau_{\rm p}$) in the range 10–100 (64–640 s), and is tidally locked. We assume the star's age lies between 2 and 8 Gyr, and Q_* (τ_*) in the range 10^5 to 10^{10} (1 to 10^{-4} s) and $t_{\rm des} = 10^8$ years. We used the same scaling relations as in Section 4. For the 0.1 $M_{\rm Sun}$ case, a was chosen in the range [0.029, 0.031] AU, for 0.15 $M_{\rm Sun}$ it was [0.055, 0.065] AU, for 0.2 $M_{\rm Sun}$ it was [0.085, 0.095] AU, and for 0.25 $M_{\rm Sun}$ it was [0.095, 0.105] AU. For each parameter the uncertainty distribution was uniform in the quoted range, except for e, which was chosen uniformly

in the range $-5 \leq \log_{10}(e) \leq -1$. We then randomly determined the system parameters in these ranges and integrated the tidal history backward in time, using the models presented in Appendix E, for the randomly chosen age of the system. We ignored the possibility of spin-orbit resonance capture, which would dramatically alter the history. For each stellar mass and tidal model, we simulated 30,000 possible configurations.

In Fig. 4, we show our results graphically. As we are considering a range of masses, we chose to represent the runaway greenhouse flux with a 2.5 $M_{\rm Earth}$ planet; that is, the solid curves show where $F_{\rm tide} = F_{\rm crit} = 309$ W m^{-2}. The three contours show the probability density for the planet's location $t_{\rm des} = 10^8$ years after the system's formation. The contours show where the probability has dropped by 50%, 90%, and 99% of the peak value; solid contours are for the CPL

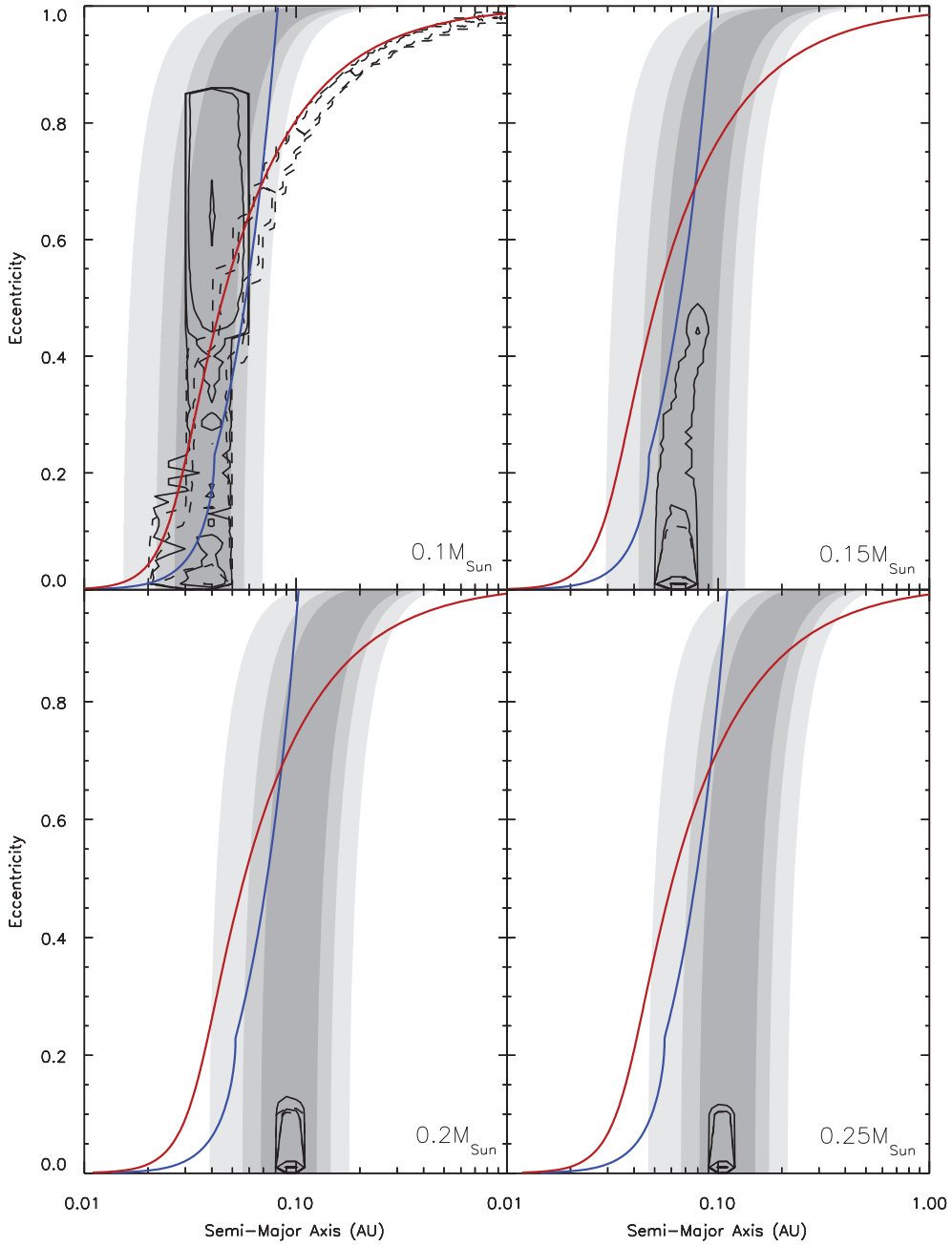

FIG. 4. Orbits of hypothetical planets around M dwarfs after $t_{\rm des}$. The top left panel is a 0.1 $M_{\rm Sun}$ star, top right 0.15 $M_{\rm Sun}$, bottom left 0.2 $M_{\rm Sun}$, and bottom right 0.25 $M_{\rm Sun}$. The grayscale represents the Selsis *et al.* (2007) IHZ boundaries with the same format as Fig. 2. For reference, the red and blue curves show the tidal greenhouse limit for a 2.5 $M_{\rm Earth}$ planet with $Q_{\rm p} = 10$ (CPL model, blue curve) or $\tau_{\rm p} = 640$ s (CTL model, red curve). Contours denote levels of constant probability density (for densities 50%, 90%, and 99% of the peak value) for the initial orbit of the planet: solid corresponds to the CPL model (compare to blue curve), dashed to CTL (compare to red curve). In the bottom two panels there has been negligible orbital evolution for either tidal model.

model, dashed for the CTL. If the probability contours intersect or even come close to the colored $F_{tide}=F_{crit}$ curves, then the planet may be a "Habitable Zone Venus," a planet that appears habitable by the IHZ metric but is probably more Venus-like than Earth-like.

The shapes of the regions in Fig. 4 are due to our parameter choices and the assumptions implicit in the two tidal models. The CPL model does not include eccentricity terms to as high an order as the CTL model; hence the CTL model predicts more evolution at large *e*. In the top left panel, this effect is seen clearly, as the most likely orbits at 100 Myr in the CPL model are at lower semimajor axis than in the CTL model. We stress that this example is purely hypothetical, and the actual shapes of the contours could be very different for actual systems.

For the 0.1 M_{Sun} case (top left), the planet may have spent enough time in the tidal greenhouse to be uninhabitable. For larger-mass stars, however, the danger of tidal desiccation is smaller. In the 0.15 M_{Sun} case, the peak in the CPL probability density at $a=0.08$, $e=0.45$ represents 1% of our simulations. Although the contours do not cross the CPL runaway greenhouse (blue) curve, they do come close; hence there is a small chance that our putative candidate is a super-Venus, especially if we allow for absorption of stellar radiation.

However, for $M_* > 0.15\ M_{Sun}$, planets with low eccentricity probably have always had low eccentricity; that is, the evolution was negligible. This sharp contrast between 0.1 and 0.2 M_{Sun} occurs because of the steep dependence of tidal heating on *a*. At larger stellar masses, the circular IHZ has been pushed away from the reach of fatal tidal heating.

This experiment is purely illustrative, with arbitrary parameters and uncertainty distributions. If a terrestrial planet was discovered in the IHZ of a very low-mass star, then this methodology could be performed in order to characterize its potential to support life. One could derive a value of t_{des} tailored to the primary and determine the probability that the planet spent more than that in a tidal greenhouse state and hence is uninhabitable. In principle, one should also allow a range of albedos and include radiation to determine the amount of time that the total surface energy flux, $F_{tot}=F_{tide}+F_{insol}$, is larger than F_{crit}; but we leave such an analysis for future work.

6. Application to Gl 667C

Two or more planets orbit the 0.3 M_{Sun} star Gl 667C (Bonfils *et al.*, 2011; Anglada-Escudé *et al.*, 2012; Delfosse *et al.*, 2012). Planets c and d appear to lie in the IHZ, while a third planet, b, lies interior. Planet c is at least 4.5 M_{Earth} and orbits near the inner edge of the IHZ. Planet d, which is weakly detected in both studies, lies near the 50% cloud cover outer boundary. At 0.23 AU, planet d is too far from the star to be subjected to strong tidal heating, at least if it is tidally locked. Anglada-Escudé *et al.* (2012) and Delfosse *et al.* (2012) proposed different solutions to the system with the former setting c's eccentricity to 0 but stating that it is only constrained to be <0.27, while the latter assign its eccentricity to be 0.34 ± 0.1. The minimum mass estimates are almost identical at 4.25 M_{Earth} (Anglada-Escudé *et al.*, 2012) and 4.5 M_{Earth} (Delfosse *et al.*, 2012). Here, we use the Anglada-Escudé *et al.* (2012) solution, but note that using data from (Delfosse *et al.*, 2012) does not change our results.

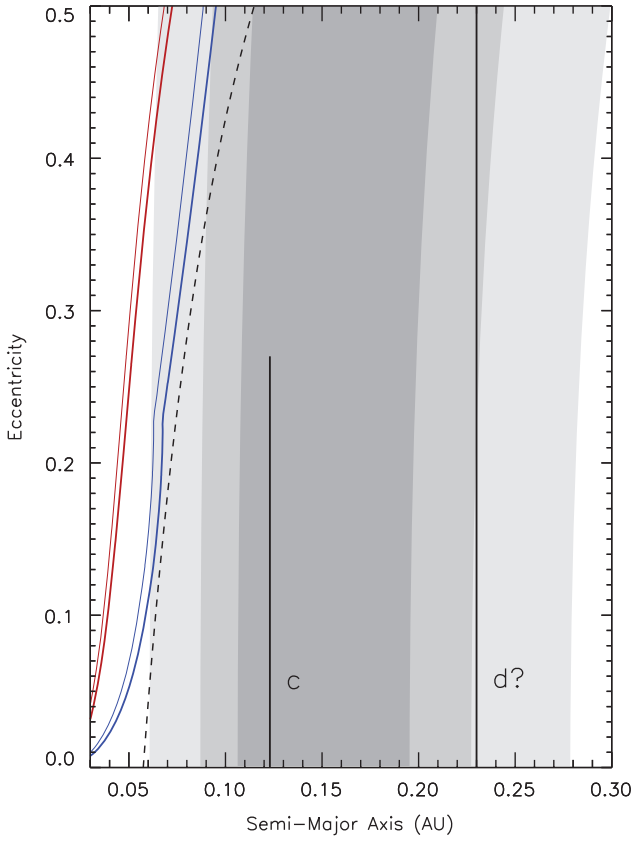

FIG. 5. Comparison of the IHZ to the tidal greenhouse limits for Gl 667C c, in a similar format as Fig. 2. Here the thin lines correspond to a 4.5 M_{Earth} planet and thick to 9 M_{Earth}. The vertical black lines correspond to the uncertainty in eccentricity of c and d (the latter's existence remains uncertain). The dashed, black curve represents where c's and b's orbits cross; hence the region to the left is dynamically unstable.

In Fig. 5, we show the system in the same format as in Fig. 2. As this planet was detected via radial velocity data, its true mass is unknown. We consider two possibilities here: an edge-on geometry in which its actual mass is 4.5 M_{Earth} and an inclined case in which its actual mass is doubled, 9 M_{Earth}. In Fig. 5, the thin lines correspond to the minimum mass, thick to twice-minimum. The vertical extent of the line corresponds to the uncertainty in eccentricity. The orbit of c is marked by the vertical black line at $a=0.123$ AU, and d at 0.23 AU.

The CTL model (red curves) barely intersects the 100% cloud cover IHZ at large *e*. The CPL model penetrates the IHZ more significantly but still does not reach the orbit of c. Thus, planet c is not currently experiencing a tidal greenhouse, assuming no obliquity and pseudo-synchronous rotation. We also see that d is completely safe from the tidal greenhouse.

But could planet c have been in the tidal greenhouse and be desiccated today? The answer is almost assuredly no. In this case, we can appeal to the orbital architecture, rather than running a suite of Monte Carlo simulations as in Section 5. The dashed, black line of Fig. 5 shows where the orbit of c crosses the orbit of b. Such a configuration is as close as the two planets could possibly be and remain stable, assuming no mean-motion resonances, which are not detected in this system (Anglada-Escudé *et al.*, 2012). This black curve is

always exterior to the tidal greenhouse curves out to the current orbit of c. Therefore, we may safely conclude that c was never in a tidal greenhouse. Furthermore, the planet should have become tidally locked within 10^7 years (Heller *et al.,* 2011), which is much less than t_{des}. Hence, any initial burst of tidal heating due to non-equilibrium rotation or obliquity was too short to sterilize this planet. Gl 667C c remains a habitable planet candidate.

7. Discussion

The previous results show where tidal heating can limit habitability for planets orbiting low-mass stars. However, many phenomena complicate the process and could alter our findings. Here, we discuss the results of the previous sections in light of our simplifying assumptions, observational requirements, and theoretical limitations.

We find that Gl 667C c probably did not lose its water to tidal heating, because interactions with other planets prevent its eccentricity from being large enough to trigger the tidal greenhouse. As more potentially habitable planets are discovered around low-mass stars, a similar analysis as in Section 5 should be undertaken in order to assess the possibility that the planet could in fact be dehydrated. As we may only be able to spectroscopically characterize a few planets with the James Webb Space Telescope (Kaltenegger and Traub, 2009; Seager *et al.,* 2009), prioritization of targets is crucial, and past and present tidal heating will help determine the best planet to observe.

The timescale for e to decay may be smaller than the timescale for *in situ* terrestrial planet formation (Lecar and Aarseth, 1986; Wetherill and Stewart, 1989; Lissauer, 1993; Kokubo and Ida, 1998; Raymond *et al.,* 2007). On the other hand, terrestrial planets could be pushed into such a position by a migrating gas giant in about that timescale (Raymond *et al.,* 2006; Mandell *et al.,* 2007). It is therefore natural to wonder whether such planets can even form, as the tidal effects could suppress planet formation or damp out the eccentricity of a protoplanet before it is massive enough to support clement conditions. Several scenarios suggest that fully formed planets can be Tidal Venuses. Orbital instabilities can excite *e.* Planet-planet scattering and divergent resonance crossing appear to play a role in sculpting many planetary systems, including our own (*e.g.,* Weidenschilling and Marzari, 1996; Tsiganis *et al.,* 2005; Nesvorný, 2011).

These phenomena can develop long after planet formation has occurred. Recently, it has been suggested that exoplanetary systems in resonance appear systematically younger than the general population, suggesting that instabilities can even occur after many billions of years (Koriski and Zucker, 2011). Therefore, we conclude that tidal greenhouses are plausible.

The role of oceans in the tidal dissipation process is clearly very important yet also very poorly understood. We have used up-to-date information regarding the dissipation of energy in Earth's ocean and assumed that terrestrial exoplanets will behave similarly, yet many issues remain outstanding. We have ignored the role of inertial waves, which provide additional heating of aqueous mantles of icy satellites (Tyler, 2008, 2011). Therefore, the tidal heating values we obtained may, in fact, be too low, further increasing the threat to habitability. Regardless, our ranges for Q or τ spanned an order of magnitude, but a wider range of values is still possible, as they are complex functions of ocean depth, ocean floor topography, and the shape of any continents or islands that may be present. As "exobathymetry" seems a distant dream, tidal dissipation in Earth-like worlds will remain mysterious for the foreseeable future.

Further complicating the situation, oceans may evaporate long before t_{des}, potentially leading to a cyclical process of evaporation and precipitation: After the oceans disappear, Q increases and the tidal heat decreases, causing the planet to drop out of the tidal greenhouse, so the water rains out, reforming the oceans and lowering Q again. Whether such a cycle exists is pure speculation, but we note that an analogous situation can occur with the classic IHZ, where evaporated water forms clouds that increase the albedo, which in turn lowers the upward long-wavelength flux from the surface, and the planet then drops out of the runaway greenhouse. Our choices for Q, τ, F_{crit}, and t_{des} can be revised as new observations provide firmer constraints. Of these, t_{des} needs the most work, as it is a function of poorly constrained host properties and challenging planetary escape processes (see, *e.g.,* Tian, 2009).

A Tidal Venus is an extreme case of tidal heating, over 2 orders of magnitude more powerful than on Io. We have therefore made a considerable extrapolation. Perhaps oceans and/or mantles adjust to the increased heating and fail to reach that flux. Our choice for Q and τ implies that most dissipation occurs in the ocean. For the solid interior, Běhounková *et al.* (2011) found that tidal heating at about F_{crit} leads to a "thermal runaway" for planets that transport internal energy through convection. Although they did not consider the possibility of advection via volcanism, the geophysics of Tidal Venuses requires closer scrutiny. We are unaware of any research exploring the physical oceanography of planets undergoing strong tidal heating, suggesting it is an interesting topic for future research.

Our treatment ignored mutual gravitational interactions between planets or large satellites, which can significantly alter the evolution. Gravitational perturbations can pump up eccentricities and obliquities to nonzero values and may be able to modify the spin period. From Fig. 2, we see that planets near the inner edge of the HZ may be in a tidal greenhouse for eccentricities less than 0.02. Other bodies in the system can easily perturb eccentricities to larger values; hence planets in multiple systems may be especially susceptible to a tidal greenhouse, as this driven eccentricity can be maintained for arbitrarily long timescales. As individual systems are discovered, this point should be revisited.

On the other hand, orbital stability arguments could allow us to preclude the tidal greenhouse in multiplanet systems, as for Gl 667C. When the eccentricity required for the tidal greenhouse is so large that the system is unstable, then one can safely exclude the Tidal Venus state. Hence, the presence of additional companions provides critical information when assessing habitability.

Many other critical phenomena were also left out, such as atmospheric erosion by flaring, stellar activity, and magnetic dynamo generation (Khodachenko *et al.,* 2007; Lammer *et al.,* 2007, 2010; Tian, 2009; Segura *et al.,* 2010; Driscoll and Olson, 2011). Tidal heating provides an interesting counterbalance to atmospheric erosion, as it may increase the outgassing rates and maintain a permanent atmosphere. The outgassing

and escape need to remain in a balance, as wild pressure and density fluctuations will undoubtedly alter the biosphere; but in principle, tidally driven outgassing could reduce the danger of atmospheric removal. On the other hand, more intense outgassing without commensurate drawdown by processes like the carbonate-silicate cycle could increase the threat of a moist greenhouse. Magnetic fields may slow down atmospheric loss, but tidal heating may decrease the dynamo. If magnetic fields are generated by convection in the outer core between a hot inner core and a cool mantle (Olson and Christensen, 2006; Driscoll and Olson, 2011), then tidal heating of the mantle may suppress magnetic field generation (Stevenson, 2010). This issue has not yet been explored for tidally heated exoplanets, but it could play a major role in habitability. Future work should couple outgassing and escape rates in order to determine how the two interact.

8. Conclusions

We have shown that tidal heating of some exoplanets may exceed the threshold of the runaway greenhouse, the traditional inner edge of the IHZ. We find that for stars with masses $< 0.3\ M_{\rm Sun}$, planets in their IHZs with low eccentricity can be uninhabitable regardless of insolation. We have thus fundamentally revised the HZ boundaries for planets on eccentric orbits. Unlike insolation from main sequence stars, tidal heating at a desiccating greenhouse level may drop off rapidly, but not so rapidly as to preclude the possibility that a planet's entire inventory of water can be lost permanently; see Fig. 3. These planets will be uninhabitable regardless of future tidal heating, that is, a planet found with minimal tidal heating today may still have experienced sufficient heating for sufficient duration to render it uninhabitable. Additional planetary companions are important: They can drive eccentricity and sustain a tidal greenhouse, or they can be used with stability arguments to rule out an early tidal greenhouse.

Traditionally, habitability models have focused on insolation, implying that the star is the most important aspect of habitability. We have shown that in some circumstances tidal effects are more important in determining the inner edge of the HZ. Planetary habitability is a function of the star, the planet, and the planetary system. The Kasting *et al.* (1993) IHZ has served well as a guide but is insufficient. Combining all the processes relevant to habitability into a single model is a daunting challenge to say the least, but a proper assessment of a planet's potential for habitability relies on a wide diversity of properties, some of which will not be observable any time soon. Nevertheless, the prospect of identifying an inhabited planet is strong motivation. Moreover, the high cost in time, money, and resources required to establish a planet as inhabited demand that we use these resources efficiently. In this study, we have compiled numerous tidal processes and empirical relationships so that at least the tidal effects predicted by linear theory may be applied to terrestrial planets in the IHZs of low-luminosity hosts.

Appendix A. Relations for the Inner Edge of the Habitable Zone

The critical flux for the runaway greenhouse depends weakly on the acceleration due to gravity, g, in the planetary atmosphere. Flux is emitted to space from the level of optical depth unity. The optical depth of a layer of absorbing gas depends to first order on the mass of the layer, so with higher g the pressure at the base of a constant mass layer will be higher. For the Simpson-Nakajima limit, the T–p structure of the atmosphere is the saturation vapor pressure curve, so higher p implies higher T and permits a higher critical flux. This positive relationship is offset to some extent by pressure-broadening of absorption, so at higher g (and higher p), less mass of water is required to provide an optical depth of unity (Pierrehumbert, 2010; Goldblatt and Watson, 2012).

Pierrehumbert (2010) derived a semi-analytical relationship for the critical flux due to the Simpson-Nakajima limit:

$$F_{crit} = A\sigma \left(\frac{l}{R \ln\left(P_* \sqrt{\frac{\kappa}{2P_0 g}} \right)} \right)^4 \tag{A1}$$

where l is the latent heat capacity of water, R is the universal gas constant, P_0 is the pressure at which the line strengths are evaluated, g is the gravitational acceleration in the planetary atmosphere. κ is a gray absorption coefficient, and A is a constant of order unity; Pierrehumbert (2010) fits these to numerical runs of a radiative transfer code with $\kappa = 0.055$ and $A = 0.7344$. P_* is a scaled pressure given by

$$P_* = P_{ref} e^{\frac{l}{RT_{ref}}} \tag{A2}$$

where $T_{\rm ref} = 273.13$ K and $P_{\rm ref} = 610.616$ Pa are points on the saturation vapor pressure curve of water, taken as the triple point. This calculated limit is shown in Fig. A1.

For convenience, we use an empirical relationship for the moist greenhouse limit derived by Selsis *et al.* (2007):

$$l_{\rm in} = (l_{\rm in,Sun} - a_{\rm in} T_* - b_{\rm in} T_*^2) \left(\frac{L_*}{L_{\rm Sun}} \right)^{1/2} \tag{A3}$$

The outer edge (not due to a desiccating greenhouse) can be expressed in a similar format as

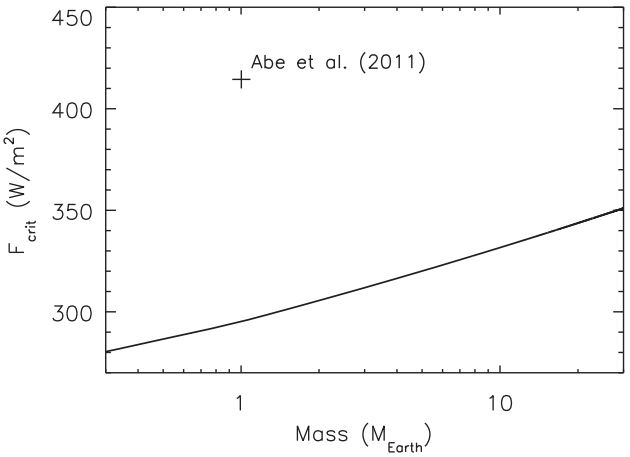

FIG. A1. Surface flux required to trigger a runaway greenhouse ($F_{\rm crit}$) as a function of planet mass. The solid line is the relation for wet planets from Pierrehumbert (2011), and the cross is the limit from Abe *et al.* (2011) for a dry planet.

$$l_{\rm out} = (l_{\rm out,Sun} - a_{\rm out} T_* - b_{\rm out} T_*^2 \left(\frac{L_*}{L_{\rm Sun}}\right)^{1/2} \quad \text{(A4)}$$

In these equations, $l_{\rm in}$ and $l_{\rm out}$ are the inner and outer edges of the IHZ, respectively, in astronomical units; $l_{\rm in,Sun}$ and $l_{\rm out,Sun}$ are the inner and outer edges of the IHZ in the solar system, respectively, in astronomical units; $a_{\rm in} = 2.7619 \times 10^{-5}$ AU/K, $b_{\rm in} = 3.8095 \times 10^{-9}$ AU/K^2, $a_{\rm out} = 1.3786 \times 10^{-4}$ AU/K, and $b_{\rm out} = 1.4286 \times 10^{-9}$ AU/K^2 are empirically determined constants; and L_* and $L_{\rm Sun}$ are the stellar and solar luminosity, respectively. $T_* = T_{\rm eff} - 5700$ K, where $T_{\rm eff}$ is the "effective temperature" of the star

$$T_{\rm eff} = \left(\frac{L_*}{4\pi R_*^2}\right)^{1/4} \quad \text{(A5)}$$

where R_* is the stellar radius and σ is the Stefan-Boltzmann constant. Usually, however, the IHZ is couched in terms of the stellar mass M_* and a; hence relationships between L_*, M_*, and R_* are needed to produce such an expression. Empirical and theoretical relations between these properties are reviewed in Appendix C.

The values of $l_{\rm in,Sun}$ and $l_{\rm out,Sun}$ are therefore the key parameters in the identification of the edges of the IHZ. We consider three criteria identified by Selsis *et al.* (2007): (1) 0% cloud cover, (2) 50% cloud cover, and (3) 100% cloud cover. Selsis *et al.* (2007) give values of $l_{\rm in,Sun}$ of 0.89, 0.72, and $\sim$0.49 AU for the three possibilities, respectively. For the outer edge, Selsis *et al.* (2007) gave values of $l_{\rm out,Sun}$ of 1.67, 1.95, and 2.4 AU for the three cloud cover models, respectively. We arbitrarily choose the 50% cloud cover case to be the limits of the IHZ. This choice is the middle of the possibilities and roughly corresponds to the cloud cover on Earth.

However, as Selsis *et al.* (2007) noted,

> the effect of the spectral type on the albedo, included in Eqs. (3–4) as a quadratic function of ($T_{\rm eff}$ – 5700), was estimated only for a cloud-free atmosphere. Since the reflectivity of clouds is less sensitive to wavelength, this quadratic term may not be valid to scale the boundaries of the HZ for planets covered by clouds.

Furthermore, the assumption that Selsis *et al.* (2007) made, that clouds do not affect the IR flux from a planet at the inner edge of the HZ, is not strong, so the cloudy results should be interpreted with caution. Furthermore, assumptions used in the models from which Selsis *et al.* (2007) derived their results assume fast planetary rotation, so it will not be a good approximation for most tidally locked exoplanets.

Figure A2 shows the range of the IHZ for the M dwarf mass range for the empirical relations presented in Appendix C. For very low-mass stars ($< 0.1\ M_{\rm Sun}$), the position of the IHZ may differ by 50% depending on the relationships invoked. However, for larger stars, the IHZ is mostly independent of the chosen mass-luminosity and mass-radius relationships.

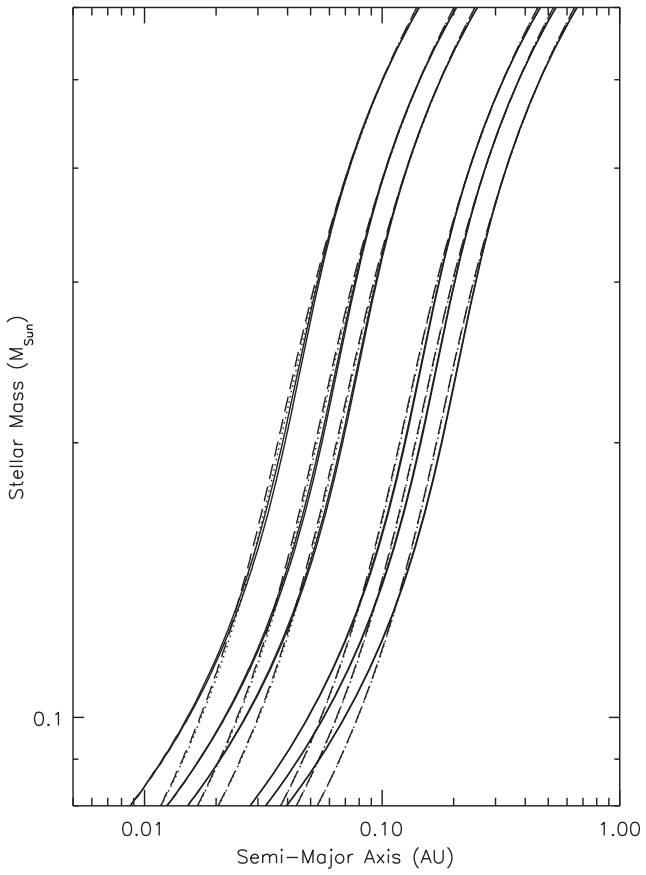

FIG. A2. IHZ boundaries for different combinations of mass-radius and mass-luminosity relations and using the three different cloud cover IHZ limits from Selsis *et al.* (2007). Except for the inner edge near $M_* = 0.2\ M_{\rm Sun}$, the effective temperature does not affect the boundaries (note the numerous curves that are visible). Six combinations are plotted, but most are invisible as they are on top of each other. At low M_*, the more interior IHZ limits assume the RH00 mass-luminosity relationship; see Appendix C.

Appendix B. The Desiccation Timescale

As discussed in Section 2, the details of mass loss on a planet near the inner edge of the HZ of a very low-mass star are largely unknown. Therefore, the timescale for desiccation is difficult to constrain. In this appendix, we describe a simple model for $t_{\rm des}$ and justify the value used in the main text of 10^8 years.

We use the atmospheric mass loss model described by Erkaev *et al.* (2007), which improves the standard model by Watson *et al.* (1981). In the Watson *et al.* picture, a layer in the atmosphere exists where absorption of high-energy photons heats the particles to a temperature that permits Jeans escape. Photons in the X-ray and XUV have the energy to drive this escape on most self-consistent atmospheres. In essence, the particles carry away the excess solar energy. Watson *et al.* (1981) calculated that Venus would lose its water in 280 Myr. The actual value is probably less than that, as they were unaware that XUV emission is larger for younger stars, as the spacecraft capable of such observations had yet to be launched. Furthermore, their model did not consider the possibility of mass loss through Lagrange points, or "Roche lobe overflow." Erkaev *et al.* (2007) provided a slight modification to the Watson *et al.*

(1981) model that accounts for this phenomenon for hot Jupiters. The physics of mass loss from a terrestrial atmosphere may be different than that on a giant, but as we are interested in objects that are experiencing tidal forces, we use the Erkaev *et al.* (2007) model,

$$\frac{dM_p}{dt} = -\frac{\pi R_x^2 R_p \varepsilon F_{XUV}}{G M_p k_{tide}} \quad \text{(B1)}$$

where R_x is the radius of the atmosphere at which the optical depth for stellar XUV photons is unity, ε is the efficiency of converting these photons into the kinetic energy of escaping particles, F_{XUV} is the incident flux of the photons. The parameter k_{tide} represents the reduction in energy required for escape of a particle due to the star's gravitational pull:

$$k_{tide} = 1 - \frac{3}{2\chi} + \frac{1}{2\chi^3} < 1 \quad \text{(B2)}$$

and

$$\chi = \left(\frac{M_p}{3M_*}\right)^3 \frac{a}{R_x} \quad \text{(B3)}$$

is the ratio of the "Hill radius" to the radius at the absorbing layer. From Eq. B1 it is trivial to show that

$$t_{des} = \frac{G M_p m_H k_{tide}}{\pi R_x^2 R_p \varepsilon F_{XUV}} \quad \text{(B4)}$$

where m_H is the total mass of all the hydrogen atoms that must be lost.

The values of F_{XUV} and ε are therefore the key parameters, as they represent the magnitude and efficiency of the process. Unfortunately, very little is known about the former for very low-mass M dwarfs with ages of a few hundred million years. The stars are very faint and, moreover, prone to flaring. However, there is a secular decrease in activity as the stars age (West *et al.*, 2008), but the data are still too sparse to allow a satisfactory fit. Recent work connected X-ray sources from space telescopes (*e.g.*, GALEX) and ground-based surveys (*e.g.*, Sloan Digital Sky Survey) and found that older low-mass stars tend to emit about 10^{-6} to 10^{-3} of their energy in the XUV in quiescence (West, personal communication). During flares, that emission can increase by an order of magnitude (Hawley and Pettersen, 1991; Kowalski *et al.*, 2012). As all stars are more active when they are young, we should expect the XUV emission to be substantially larger at those times.

The value of ε must be less than 1, as not all the absorbed energy removes particles. Observations of hot Jupiters suggest values of ε of 0.4 (Yelle, 2004; Lammer *et al.*, 2009; Jackson *et al.*, 2010), while on Venus $\varepsilon \sim 0.15$ (Chassefière, 1996). However, our model also requires these photons to dissociate the water molecules, hence we should expect ε on a Tidal Venus to be much less than on a hot Jupiter with a predominantly hydrogen atmosphere. For reference, using the assumptions of Watson *et al.* (1981), we find $\varepsilon = 1.7 \times 10^{-4}$ implies $t_{des} = 280$ Myr for Venus.

In Fig. B1, we show the desiccation timescale for an Earth-like planet orbiting a 0.1 M_{Sun} star at 0.03 AU for a range of XUV luminosities and ε. The initial mass of the planet in hydrogen is 1.4×10^{-5} M_{Earth}, the current value of Earth and the same value used by Watson *et al.* (1981), and $R_x = 1.02$ R_p. The luminosity of the star is 0.0008 L_{Sun}, and the planet lies inside the 0% cloud cover HZ (see Appendix A). The contour lines show $\log_{10}(t_{des})$. For $\varepsilon \sim 10^{-4}$, a few percent of the luminosity would need to be in the XUV for t_{des} to be 10^8 years, while hot Jupiter escape rates would only require $> 10^{-5}$ of the luminosity to be in the XUV.

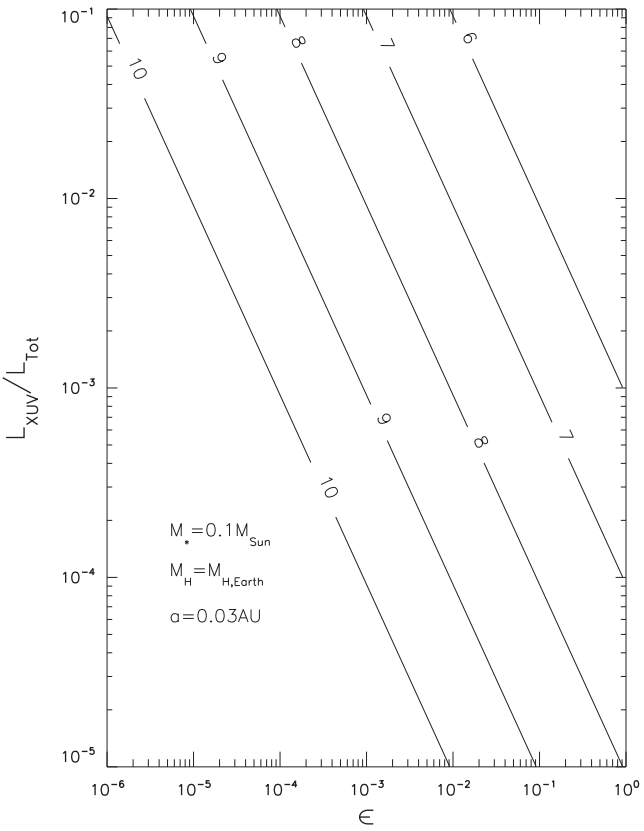

FIG. B1. Desiccation timescale for an Earth-like planet orbiting a 0.1 M_{Sun} star as a function of the fraction of the luminosity in the XUV and the efficiency of converting that energy into escaping particles. Contour lines are $\log_{10}(t_{des}/\text{yr})$. The planet initially has the same water mass fraction as the Earth and a semimajor axis of 0.03 AU.

The environment near a forming star is very energetic; therefore we should expect other phenomena, such as ablation and magnetic fields, also erode the atmosphere. Therefore, the actual values of t_{des} are assuredly shorter than those presented in Fig. B1. We conclude that $t_{des} = 100$ Myr is a reasonable choice, while explicitly acknowledging a large range is possible. Finally, we note that simulations should couple the evolution of the XUV output to the tidal orbital evolution of the planet in order to calculate t_{des} for a given system. Jackson *et al.* (2010) created such a model for CoRoT-7 b (Léger *et al.*, 2009), which orbits close to a solar-mass star. For such stars the generic evolution of their XUV evolution is known (Ribas *et al.*, 2005); hence such an analysis was quite revealing. Given the poor constraints on XUV evolution for M dwarfs, we eschewed such coupling, deferring that analysis to future work.

Appendix C. Masses, Radii, and Luminosities of M Dwarfs

In this appendix, we review relationships between mass, radius, luminosity, and effective temperature for M dwarfs ($M_* \leq 0.6\ M_{\rm Sun}$), and their effects on the limits of the IHZ. Measurements of these fundamental stellar properties are challenging, and several studies have produced empirical and theoretical relations.

We first consider the mass-radius relation. We include empirical models by Gorda and Svechnikov (1999) (GS99), Reid and Hawley (2000) (RH00), Bayless and Orosz (2006) (BO06), as well as the theoretical models of Baraffe *et al.* (1998) (B98). This latter model is parameterized in terms of the metallicity as defined by astronomers:

$$[\mathrm{Fe/H}] \equiv \log_{10}[\mathrm{Fe/H}]_* - \log_{10}[\mathrm{Fe/H}]_{\rm Sun} \tag{C1}$$

in other words, it is the difference between the ratio of iron to hydrogen in a star to that of the Sun. B98 consider solar metallicity stars ([Fe/H] = 0) and subsolar ([Fe/H] = −0.5). GS99 and BO06 present analytic fits that are shown in Table C1. For RH00, we take their data in Table 4.1 and derive a third-order polynomial fit, $y = b_0 + b_1 x + b_2 x^2 + b_3 x^3$, using a Levenberg-Marquardt minimization scheme, and present the results in Table C1. The top two panels of Fig. C1 show the relationships graphically.

Next, we examine the mass-luminosity relationships detailed in RH00, Scalo *et al.* (2007) (S07) and B98. For the former, we again fit their data with a third-order polynomial. The fits are listed in Table C1 and shown graphically in the bottom panels of Fig. C1.

Appendix D. Radii of Terrestrial Planets

In this appendix, we review published studies that provide analytic formulae relating terrestrial planet mass and radius. Throughout the study, we appealed to the relationship derived by Sotin *et al.* (2007), who considered two types of planets: Earth-like composition and "ocean planets" that are 50% H_2O by weight. The scaling relationship for the former is

$$\frac{R_{\rm p}}{R_{\rm Earth}} = \begin{cases} \left(\frac{M_{\rm p}}{M_{\rm Earth}}\right)^{0.306} & 10^{-2} M_{\rm Earth} < M_{\rm p} < 1 M_{\rm Earth} \\ \left(\frac{M_{\rm p}}{M_{\rm Earth}}\right)^{0.274} & 1 M_{\rm Earth} < M_{\rm p} < 10\ M_{\rm Earth} \end{cases} \tag{D1}$$

and for the latter

$$\frac{R_{\rm p}}{R_{\rm Earth}} = \begin{cases} 1.258\left(\frac{M_{\rm p}}{M_{\rm Earth}}\right)^{0.302} & 10^{-2} M_{\rm Earth} < M_{\rm p} < 1 M_{\rm Earth} \\ 1.262\left(\frac{M_{\rm p}}{M_{\rm Earth}}\right)^{0.275} & 1 M_{\rm Earth} < M_{\rm p} < 10\ M_{\rm Earth} \end{cases} \tag{D2}$$

Fortney *et al.* (2007) parameterized the radii ($M_{\rm p} > 0.01\ M_{\rm Earth}$) in terms of the ratio of ice to rock, $f_{\rm ice}$, or rock to iron, $f_{\rm rock}$. They assumed that these two combinations are the most likely for terrestrial exoplanets and derived the following relationships:

$$\begin{aligned} \frac{R_{\rm p}}{R_{\rm Earth}} = {} & (0.0912\, f_{\rm ice} + 0.1603)\left(\log_{10}\frac{M_{\rm p}}{M_{\rm Earth}}\right)^2 \\ & + (0.330\, f_{\rm ice} + 0.7387)\log_{10}\frac{M_{\rm p}}{M_{\rm Earth}} \\ & + 0.4639\, f_{\rm ice} + 1.1193 \end{aligned} \tag{D3}$$

and

$$\begin{aligned} \frac{R_{\rm p}}{R_{\rm Earth}} = {} & (0.0592\, f_{\rm rock} + 0.0975)\left(\log_{10}\frac{M_{\rm p}}{M_{\rm Earth}}\right)^2 \\ & + (0.2337\, f_{\rm rock} + 0.4938)\log_{10}\frac{M_{\rm p}}{M_{\rm Earth}} \\ & + 0.3102\, f_{\rm rock} + 0.7932 \end{aligned} \tag{D4}$$

In these equations, $f_{\rm ice} = 1$ corresponds to a pure water, $f_{\rm ice} = 0$ and $f_{\rm rock} = 1$ to a pure rock (silicate) planet, and $f_{\rm rock} = 0$ is a planet made of pure iron. Note that Eqs. D3–D4 are analytic fits to complex models and, hence, predict slightly different values for $R_{\rm p}$ for a planet made of rock ($f_{\rm ice} = 0$ and $f_{\rm rock} = 1$).

Table C1. Scaling Relations for M Dwarfs

x	y	b_0	b_1	b_2	b_3	χ^2	*Ref.*
$\log_{10}(M_*/M_{\rm Sun})$	$\log_{10}(R_*/R_{\rm Sun})$	0.1	1.03	0	0	n/a	GS99
$\log_{10}(M_*/M_{\rm Sun})$	$\log_{10}(R_*/R_{\rm Sun})$	0.0128	2.185	3.1349	1.903	0.0136	RH00
$M_*/M_{\rm Sun}$	$R_*/R_{\rm Sun}$	0.0324	0.9343	0.0374	0	n/a	BO06
$\log_{10}(M_*/M_{\rm Sun})$	$\log_{10}(R_*/R_{\rm Sun})$	0.0372	1.5	1.09	0.5361	1.72×10^{-4}	B98([Fe/H] = 0)
$\log_{10}(M_*/M_{\rm Sun})$	$\log_{10}(R_*/R_{\rm Sun})$	0.0664	1.685	1.398	0.7139	4.38×10^{-4}	B98([Fe/H] = − 0.5)
$\log_{10}(R_*/R_{\rm Sun})$	$\log_{10}(M_*/M_{\rm Sun})$	−0.0971	0.971	-2.501×10^{-5}	-1.34×10^{-5}	1.2×10^{-10}	GS99
$\log_{10}(R_*/R_{\rm Sun})$	$\log_{10}(M_*/M_{\rm Sun})$	0.1424	1.568	−0.2342	−0.5581	0.0331	RH00
$R_*/R_{\rm Sun}$	$M_*/M_{\rm Sun}$	−0.03477	1.071	-8.171×10^{-4}	−0.0412	2.83×10^{-9}	BO06
$\log_{10}(R_*/R_{\rm Sun})$	$\log_{10}(M_*/M_{\rm Sun})$	−0.03	0.507	−1.156	−0.5978	8.88×10^{-4}	B98([Fe/H] = 0)
$\log_{10}(R_*/R_{\rm Sun})$	$\log_{10}(M_*/M_{\rm Sun})$	−0.0406	0.4537	−1.211	−0.6427	0.00139	B98([Fe/H] = −0.5)
$\log_{10}(M_*/M_{\rm Sun})$	$\log_{10}(L_*/L_{\rm Sun})$	0.2984	8.7116	11.562	6.241	0.0155	RH00
$\log_{10}(M_*/M_{\rm Sun})$	$\log_{10}(L_*/L_{\rm Sun})$	0.065	7.108	8.162	4.101	n/a	S07
$\log_{10}(M_*/M_{\rm Sun})$	$\log_{10}(L_*/L_{\rm Sun})$	0.0182	7.228	9.357	5.281	0.039	B98([Fe/H] = 0)
$\log_{10}(M_*/M_{\rm Sun})$	$\log_{10}(L_*/L_{\rm Sun})$	0.4377	8.908	12.21	6.896	0.094	B98([Fe/H] = −0.5)
$\log_{10}(L_*/L_{\rm Sun})$	$\log_{10}(M_*/M_{\rm Sun})$	−0.3076	−0.5	−0.4504	−0.06852	0.00287	RH00
$\log_{10}(L_*/L_{\rm Sun})$	$\log_{10}(M_*/M_{\rm Sun})$	−0.3536	−0.5463	−0.4422	−0.06243	0.224	S07
$\log_{10}(L_*/L_{\rm Sun})$	$\log_{10}(M_*/M_{\rm Sun})$	−0.04	−0.114	−0.2765	−0.045	0.039	B98([Fe/H] = 0)
$\log_{10}(L_*/L_{\rm Sun})$	$\log_{10}(M_*/M_{\rm Sun})$	−0.03	0.00509	−0.2135	−0.0368	0.0145	B98([Fe/H] = −0.5)

n/a means χ^2 values are not available. Only reprinted are fits that were derived in the stated work.

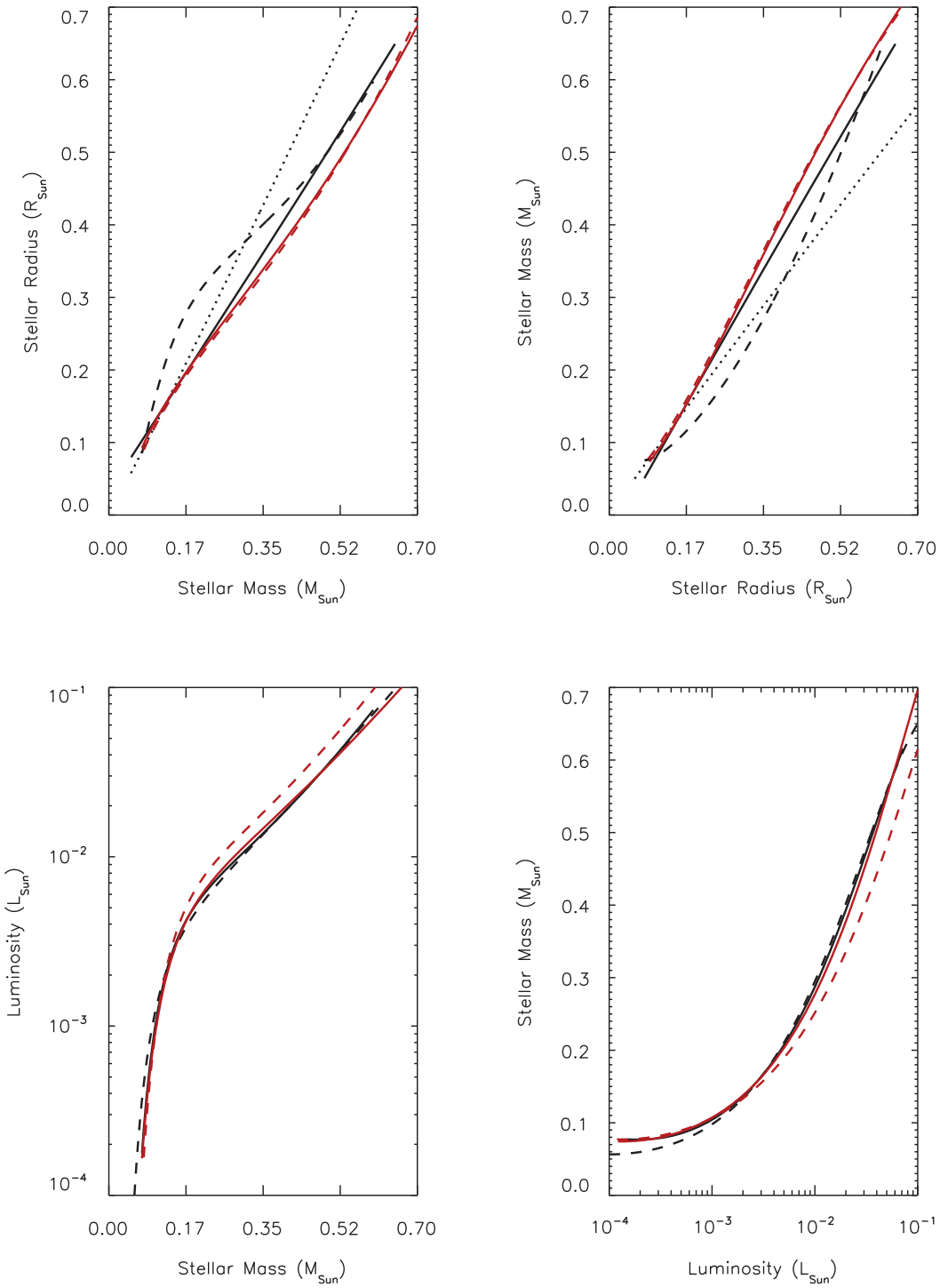

FIG. C1. Scaling relations for M dwarfs. *Top:* Mass-radius relations. Black curves are empirical relations: solid from BO06, dashed from RH00, and dotted from GS99. Red curves are theoretical curves from B98: solid assumes [Fe/H] = 0, dashed [Fe/H] = −0.5. *Bottom:* Mass-luminosity relations. Black curves are empirical relations: solid from RH00 and dotted from S07. Red curves are theoretical curves from B98: solid assumes [Fe/H] = 0, dashed [Fe/H] = −0.5.

Earth has $f_{\rm rock} = 0.67$; hence Eq. D4 becomes $R_{\rm p}/R_{\rm Earth} = 0.1372[\log_{10}(M_{\rm p}/M_{\rm Earth})]^2 + 0.6504\ \log_{10}(M_{\rm p}/M_{\rm Earth}) + 1.0010$.

Valencia *et al.* (2007) considered planets in the range 1–10 $M_{\rm Earth}$ and parameterized the radius in terms of $f_{\rm ice}$ (see also Valencia *et al.*, 2010). They found

$$\frac{R_{\rm p}}{R_{\rm Earth}} = (1 + 0.56\, f_{\rm ice}) \frac{M_p}{M_{\rm Earth}}^{0.262(1 - 0.138\, f_{\rm ice})} \quad \text{(D5)}$$

Seager *et al.* (2007) considered a wide range of planetary compositions and developed a general, but complicated,

mass-radius relationship. Although they developed several formulae, here we only present one. They found that by casting M_p and R_p in terms of "scaling values," all planets follow the relationship

$$\log_{10} r_s = k_1 + k_2 \log_{10} m_s - k_2 m_s^{k_3} \quad \text{(D6)}$$

where $k_1 = -0.20945$, $k_2 = 0.0804$, and $k_3 = 0.394$. The parameters m_s and r_s are the scaled mass and radii, respectively, and are defined as $m_s = m/m_1$ and $r_s = r/r_1$, where the denominators are a scaling factor that depends on composition and thermal effects. We will consider four compositions. For pure iron planets, $m_1 = 5.8\ M_{Earth}$ and $r_1 = 2.52\ R_{Earth}$. For pure rock (perovskite) planets, $m_1 = 10.55\ M_{Earth}$ and $r_1 = 3.9\ R_{Earth}$. For pure water planets, $m_1 = 5.52\ M_{Earth}$ and $r_1 = 4.43\ R_{Earth}$. Finally, for an Earth-like planet (30% iron, 70% perovskite), $m_1 = 6.41\ M_{Earth}$ and $r_1 = 2.84\ R_{Earth}$. Note that this formulation is only valid for $m_s < 4$.

The last relationship we review is that of Grasset *et al.* (2009), who cast their model in terms only of f_{ice}. Their formulation is complicated, and rather than reproduce it here, the reader is referred to their paper. We do not include the recent models put forth by Swift *et al.* (2012), as they did not include formulae, but they did find that their results are consistent with those of Fortney *et al.* (2007) and Valencia *et al.* (2010) for rock and iron planets.

In Fig. D1, we compare these relationships for 0.3–30 M_{Earth} and for a variety of compositions. Not all the relationships span that mass range, nor do they encompass all compositions. Furthermore, although we group planets into four types, not all types are identical. For example, we labeled the Sotin *et al.* (2007) ocean planet as a "Water" planet, but it is only 50% water, while the other three are 100% water. Nonetheless, the plot shows that if only mass is known, the radius of a planet can only be known to a factor of 2–2.5 (of course, its terrestrial nature is also unlikely to be known). As tidal heating scales as R^5, this translates to a difference in heating of 30–100, assuming identical Q or τ. Note that the solid red curve [Earth-like planet from Sotin *et al.* (2007)] has a typical shape for its class; hence the results presented here do not vary much if a different model is chosen, unless a significantly different composition is invoked.

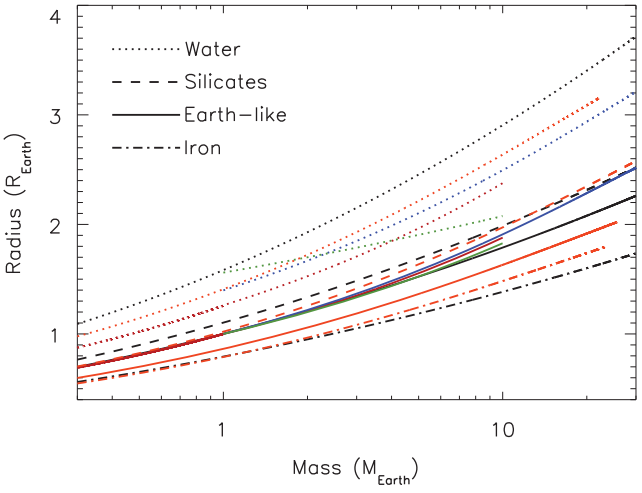

FIG. D1. Mass-radius relationships for terrestrial planets of varying compositions. Solid curves assume a roughly Earth-like composition, dashed are all silicates, dotted are at least half water, and dot-dashed are pure iron. Black correspond to Fortney *et al.* (2007), red to Sotin *et al.* (2007), blue to Grasset *et al.* (2009), green to Valencia *et al.* (2007), and orange to Seager *et al.* (2007).

Appendix E. Tidal Theory

For our calculations of tidal evolution, we employ "equilibrium tide" models, originally conceived by Darwin (1880). This model assumes the gravitational potential of the tide raiser can be expressed as the sum of Legendre polynomials (*i.e.*, surface waves) and that the elongated equilibrium shape of the perturbed body is slightly misaligned with respect to the line which connects the two centers of mass. This misalignment is due to dissipative processes within the deformed body and leads to a secular evolution of the orbit as well as the spin angular momenta of the two bodies. As described below, this approach leads to a set of six coupled, nonlinear differential equations, but note that the model is, in fact, linear in the sense that there is no coupling between the surface waves which sum to the equilibrium shape. A substantial body of research is devoted to tidal theory (*e.g.*, Hut, 1981; Ferraz-Mello *et al.*, 2008; Wisdom, 2008; Efroimsky and Williams, 2009; Leconte *et al.*, 2010), and the reader is referred to these studies for a more complete description of the derivations and nuances of tidal theory. For this investigation, we will use the models and nomenclature of Heller *et al.* (2011), which are presented below.

E.1. The constant phase lag model

In the CPL model of tidal evolution, the angle between the line connecting the centers of mass and the tidal bulge is assumed to be constant. This approach has the advantage of being analogous to a damped driven harmonic oscillator, a well-studied system, and is quite commonly utilized in planetary studies (*e.g.*, Goldreich and Soter, 1966; Greenberg, 2009). In this case, the evolution is described by the following equations:

$$\frac{de}{dt} = -\frac{ae}{8GM_1M_2}\sum_{i=1}^{2} Z_i'\left(2\varepsilon_{0,i} - \frac{49}{2}\varepsilon_{1,i} + \frac{1}{2}\varepsilon_{2,i} + 3\varepsilon_{5,i}\right) \quad \text{(E1)}$$

$$\frac{da}{dt} = \frac{a^2}{4GM_1M_2}\sum_{i=1}^{2} Z_i'(4\varepsilon_{0,i} + e^2[-20\varepsilon_{0,i} + \frac{147}{2}\varepsilon_{1,i} + \frac{1}{2}\varepsilon_{2,i} - 3\varepsilon_{5,i}] - 4\sin^2(\psi_i)[\varepsilon_{0,i} - \varepsilon_{8,i}]) \quad \text{(E2)}$$

$$\frac{d\psi_i}{dt} = \frac{Z_i' \sin(\psi_i)}{4M_i r_{g,i}^2 R_i^2 n\omega_i}([1-\xi_i]\varepsilon_{0,i} + [1+\xi_i]\{\varepsilon_{8,i} - \varepsilon_{9,i}\}) \quad \text{(E3)}$$

$$\frac{d\omega_i}{dt} = -\frac{Z_i'}{8M_i r_{g,i}^2 R_i^2 n}(4\varepsilon_{0,i} + e^2[-20\varepsilon_{0,i} + 49\varepsilon_{1,i} + \varepsilon_{2,i}] + 2\sin^2(\psi_i)[-2\varepsilon_{0,i} + \varepsilon_{8,i} + \varepsilon_{9,i}]) \quad \text{(E4)}$$

where e is eccentricity, t is time, a is semimajor axis, G is Newton's gravitational constant, M_1 and M_2 are the two masses, R_1 and R_2 are the two radii, ω_i are the rotational

frequencies, ψ_i are the obliquities, and n is the mean motion. The quantity Z' is

$$Z_t' \equiv 3G^2 k_{2,i} M_j^2 (M_i + M_j) \frac{R_i^5}{a^9} \frac{1}{nQ_i} \tag{E5}$$

where $k_{2,i}$ are the Love numbers of order 2 and Q_i are the "tidal quality factors." The parameter ξ_i is

$$\xi_i \equiv \frac{r_{g,i}^2 R_i^2 \omega_i a n}{G M_j} \tag{E6}$$

where i and j refer to the two bodies and r_g is the "radius of gyration"; that is, the moment of inertia is $M(r_g R)^2$. The signs of the phase lags are

$$\begin{aligned} \varepsilon_{0,i} &= \Sigma(2\omega_i - 2n) \\ \varepsilon_{1,i} &= \Sigma(2\omega_i - 3n \\ \varepsilon_{2,i} &= \Sigma(2\omega_i - n) \\ \varepsilon_{5,i} &= \Sigma(n) \\ \varepsilon_{8,i} &= \Sigma(\omega_i - 2n) \\ \varepsilon_{9,i} &= \Sigma(\omega_i) \end{aligned} \tag{E7}$$

with $\Sigma(x)$ the sign of any physical quantity x, thus $\Sigma(x) = +1 \vee -1 \vee 0$.

The tidal heating of the i^{th} body is due to the transformation of rotational and/or orbital energy into frictional heating. The heating from the orbit is

$$\begin{aligned} \dot{E}_{\text{orb},i} = \frac{Z_i'}{8} \times (4\varepsilon_{0,i} + e^2[-20\varepsilon_{0,i} + \frac{147}{2}\varepsilon_{1,i} \\ + \frac{1}{2}\varepsilon_{2,i} - 3\varepsilon_{5,i}] - 4\sin^2(\psi_i)[\varepsilon_{0,i} - \varepsilon_{8,i}]) \end{aligned} \tag{E8}$$

and that from the rotation is

$$\begin{aligned} \dot{E}_{\text{rot},i} = -\frac{Z_i'}{8}\frac{\omega_i}{n} \times (4\varepsilon_{0,i} + e^2[-20\varepsilon_{0,i} + 49\varepsilon_{1,i} + \varepsilon_{2,i}] \\ + 2\sin^2(\psi_i)[-2\varepsilon_{0,i} + \varepsilon_{8,i} + \varepsilon_{9,i}]) \end{aligned} \tag{E9}$$

The total heat in the i^{th} body is therefore

$$\dot{E}_{\text{tide},i}^{\text{CPL}} = -(\dot{E}_{\text{orb},i} + \dot{E}_{\text{rot},i}) > 0 \tag{E10}$$

The rate of evolution and amount of heating are set by three free parameters: Q, k_2, and r_g. We discuss the ranges of these parameters below in Appendix E.4.

Goldreich (1966) suggested that the equilibrium rotation period for both bodies is

$$P_{\text{eq}}^{\text{CPL}} = \frac{P}{1 + 9.5e^2} \tag{E11}$$

Murray and Dermott (1999) presented a derivation of this expression, which assumes the rotation rate may take a continuum of values. However, the CPL model described above only permits four "tidal waves" and, hence, does not permit this continuum. In Fig. E1, we compare Eq. E11 to the equilibrium values predicted by Eqs. E1–E4 as a function of eccentricity for Gl 581 d, that is, an orbital period of 66 days, a mass of 5.6 M_{Earth}, and a radius of 1.6 R_{Earth} (Mayor *et al.*, 2009). As expected, E7 predicts a continuous range of periods, whereas our model (solid curve) does not. The jump at $e = \sqrt{1/19}$ occurs at the $\omega/n = 1.5$ transition and nearly reaches the value predicted by Eq. E11. The next phase jump at $e = \sqrt{1/19} \approx 0.32$ is not included in the CPL model; hence it breaks down at larger values. However, at larger e values, coupling between waves and other nonlinear effects may dampen the role of tides. Therefore, the evolution at larger e predicted by the CPL model may not be qualitatively correct. We urge caution when interpreting CPL results above $e = 0.32$.

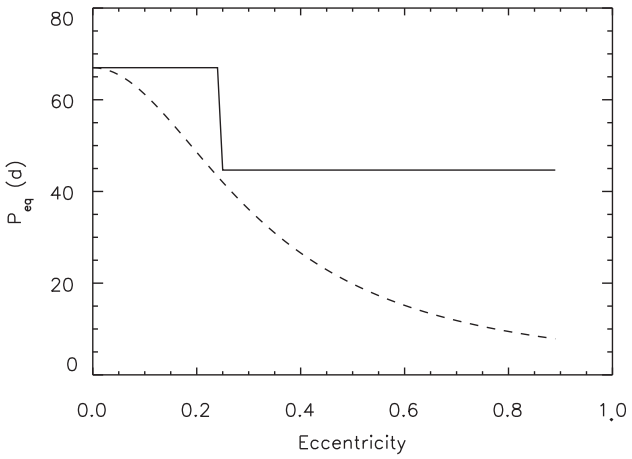

FIG. E1. Comparison of the equilibrium spin periods in the CPL framework. The solid line is the value predicted by our model, Eqs. E1–E4, the dashed is the "continuous" model of Goldreich (1966).

Thus, the CPL model can be considered from two perspectives. When modeling the evolution of a system, one should use the discrete spin values for self-consistency, that is, as an initial condition, or if forcing the spin to remain tidally locked. However, if calculating the equilibrium spin period separately, the continuous value of Eq. E7 should be used. We refer to these rotations as "discrete states" and the "continuous state." Note that this point marks a difference between our implementation of the CPL model and that described by Heller *et al.* (2011).

E.2. The constant time lag model

The CTL model assumes that the time interval between the passage of the perturber and the tidal bulge is constant. This assumption allows the tidal response to be continuous over a wide range of frequencies, unlike the CPL model. But, if the phase lag is a function of the forcing frequency, then the system is no longer analogous to a damped driven harmonic oscillator. Therefore, this model should only be used over a narrow range of frequencies (see Greenberg, 2009). However, this model's use is widespread, especially at high e, so we use it to evaluate tidal effects as well. This model predicts larger tidal heating and evolution rates at high e as any coupling between tidal waves is ignored. Therefore, the CPL and CTL models probably bracket the actual evolution.

The evolution is described by the following equations:

$$\frac{de}{dt} = \frac{11ae}{2GM_1M_2}\sum_{i=1}^{2} Z_i\left(\cos(\psi_i)\frac{f_4(e)}{\beta^{10}(e)}\frac{\omega_i}{n} - \frac{18}{11}\frac{f_3(e)}{\beta^{13}(e)}\right) \quad \text{(E12)}$$

$$\frac{da}{dt} = \frac{2a^2}{GM_1M_2}\sum_{i=1}^{2} Z_i\left(\cos(\psi_i)\frac{f_2(e)}{\beta^{12}(e)}\frac{\omega_i}{n} - \frac{f_1(e)}{\beta^{15}(e)}\right) \quad \text{(E13)}$$

$$\frac{d\psi_i}{dt} = \frac{Z_i\sin(\psi_i)}{2M_i r_{g,i}^2 R_i^2 n\omega_i}\left(\left[\cos(\psi_i) - \frac{\xi_i}{\beta}\right]\frac{f_5(e)}{\beta^9(e)}\frac{\omega_i}{n} - 2\frac{f_2(e)}{\beta^{12}(e)}\right) \quad \text{(E14)}$$

$$\frac{d\omega_i}{dt} = \frac{Z_i}{2M_i r_{g,i}^2 R_i^2 n}\left(2\cos(\psi_i)\frac{f_2(e)}{\beta^{12}(e)} - \left[1+\cos^2(\psi)\right]\frac{f_5(e)}{\beta^9(e)}\frac{\omega_i}{n}\right) \quad \text{(E15)}$$

where

$$Z_i \equiv 3G^2 k_{2,i} M_j^2 (M_i + M_j)\frac{R_i^5}{a^9}\tau_i \quad \text{(E16)}$$

and

$$\begin{aligned}
\beta(e) &= \sqrt{1-e^2}\\
f_1(e) &= 1 + \frac{31}{2}e^2 + \frac{255}{8}e^4 + \frac{185}{16}e^6 + \frac{25}{64}e^8\\
f_2(e) &= 1 + \frac{15}{2}e^2 + \frac{45}{8}e^4 + \frac{5}{16}e^6\\
f_3(e) &= 1 + \frac{15}{4}e^2 + \frac{15}{8}e^4 + \frac{5}{64}e^6\\
f_4(e) &= 1 + \frac{3}{2}e^2 + \frac{1}{8}e^4\\
f_5(e) &= 1 + 3e^2 + \frac{3}{8}e^4
\end{aligned} \quad \text{(E17)}$$

The tidal heating of the i^{th} body is therefore

$$\begin{aligned}
\dot{E}_{\text{tide},i}^{\text{CTL}} = Z_i\Bigg(&\frac{f_1(e)}{\beta^{15}(e)} - 2\frac{f_2(e)}{\beta^{12}(e)}\cos(\psi_i)\frac{\omega_i}{n}\\
&+ \left[\frac{1+\cos^2(\psi_i)}{2}\right]\frac{f_5(e)}{\beta^9(e)}\left(\frac{\omega_i}{n}\right)^2\Bigg)
\end{aligned} \quad \text{(E18)}$$

Note that Eqs. E6 and E14 include terms due to both rotation and obliquity, which were not discussed in the main text. Should information regarding these parameters become available for particular planets, they should be included in estimates of tidal heating and habitability.

It can also be shown that the equilibrium rotation period of each body is

$$P_{\text{eq}}^{\text{CTL}}(e,\psi) = P\frac{\beta^3 f_5(e)(1+\cos^2\psi)}{2f_2(e)\cos\psi} \quad \text{(E19)}$$

which for low e and $\psi = 0$ reduces to

$$P_{\text{eq}}^{\text{CTL}} = \frac{P}{1+6e^2} \quad \text{(E20)}$$

There is no general conversion between Q_{p} and τ_{p}. Only if $e = 0$ and $\psi_{\text{p}} = 0$, when merely a single tidal lag angle ε_{p} exists, then

$$Q_{\text{p}} \approx 1/(2|n - \omega_{\text{p}}|\tau_{\text{p}}) \quad \text{(E21)}$$

as long as $n - \omega_{\text{p}}$ remains unchanged. Hence, a dissipation value for an Earth-like planet of $Q_{\text{p}} = 100$ is not necessarily equivalent to a tidal time lag of 638 s, so the results for the tidal evolution will intrinsically differ between the CPL and the CTL model. However, both choices are common for the respective model.

E.3. Numerical methods

The rates of change of the six parameters affected by tidal theory are all different. The orbital parameters tend to evolve several orders of magnitude more slowly than the planetary spin parameters, at least for the cases we are interested in. Therefore, we implement a dynamical time-step scheme in our integration of tidal evolution. At the beginning of each time step, we calculate the derivatives and set the time step to

$$\Delta t = \eta \times \min\left(\frac{a}{da/dt}, \frac{e}{de/dt}, \frac{\omega_*}{d\omega_*/dt}, \frac{\psi_*}{d\psi_*/dt}, \frac{\omega_p}{d\omega_p/dt}, \frac{\psi_p}{d\psi_p/dt}\right) \quad \text{(E22)}$$

where η is a constant, which we set to 0.01. We find that larger values of η, even up to unity, produce results similar with $\eta = 0.01$, but at our more conservative choice, we find almost no difference with even smaller value of η; that is, the solution has converged. This implementation increases the speed of the code by several orders of magnitude in some cases. For example, if considering a planet with spin properties similar to Earth at 0.01 AU, the timescale to damp out the obliquity is of order years, but the orbit evolves in millions of years (depending on e). Integrating this system for billions of years with a fixed time step chosen to resolve the obliquity evolution will take many orders of magnitude more time than using this scheme. Dynamical time stepping is especially important for planets that merge with their host star (Jackson *et al.*, 2009; Levrard *et al.*, 2009).

In many cases, e and ψ can damp to arbitrarily small values; hence de/dt and $d\psi/dt$ take on meaningless values. In some cases, their respective timescales as defined above can become very short, even though they are effectively 0. This situation destroys the speed advantage gained by utilizing E18. We therefore set a floor for these values at 10^{-10}. When they reach this level, we set them to 0 and do not include them in the determination of Δt.

Finally, care must be taken as a planet approaches tidal locking. In many cases, an integration will bounce back and forth above and below the equilibrium period. This possibility is a natural result of the discrete nature of numerical integration but, again, can diminish the benefits of a dynamical time step. Therefore, if a planet comes within 10% of the equilibrium period, we set the spin period to the equilibrium value. If the orbit is eccentric and evolving, after tidal locking, we force the planet to remain locked; that is, the spin period obeys Eq. E11 or E20.

E.4. Tidal response in celestial bodies

Exoplanets are expected to have an even wider diversity of compositions and structures than those in our solar system (see Léger *et al.,* 2004; Raymond *et al.,* 2004; O'Brien *et al.,* 2006; Bond *et al.,* 2010); thus their response to tidal processes probably varies greatly. We therefore choose to keep our model simple and set $k_2 = r_g = 0.5$ for all planets.

Earth is the only body in the Solar System with a significant amount of water on its surface and is also the planet with the most detailed picture of its tidal processes. The majority of tidal dissipation on Earth occurs in the oceans, and we assume the same will occur on terrestrial exoplanets. Tidal dissipation in Earth's ocean was directly measured from TOPEX and Poseidon satellite data by Egbert and Ray (2000), who found that 50–75% of dissipation occurs in and around shallow seas, with the remainder in the open ocean, presumably due to turbulence caused by topography. Recent computer simulations have successfully reproduced this observation (Jayne, 2001; Nycander, 2005; Kelly *et al.,* 2010). For a more complete treatment of this process, consult the work of Garrett and Kunze (2007). Therefore, dissipation in planetary oceans is a complex function of continental shapes, seafloor topography, and the forcing frequency.

Lunar Laser Ranging, in which the timing of laser pulses bounced off the Moon is measured, has provided very precise measurements of the rate of the Moon's recession from Earth (Dickey *et al.,* 1994). If this recession is due only to tidal dissipation within Earth, then Earth's tidal quality factor is $Q_{\rm Earth} = 12$ (Yoder, 1995). This value is lower than most measurements in the Solar System, which are more uncertain (see below). However, given the presence of surface oceans, this extra dissipation should be expected. On the other hand, extrapolating backward from the current orbital expansion rate and employing the CPL model, one finds the Moon was at Earth's surface ~ 2 Gyr ago (MacDonald, 1964). The moon-forming impact has been dated to about 4.5 Gyr ago; hence Earth's current Q appears too low. This discrepancy may be explained by four possibilities: (1) The current Q is anomalously low, and in the past different continental configurations and/or ocean floor topography did not permit such a high dissipation; (2) The tidal effects are a function of frequency, and as Earth's rotation has slowed, the dissipation rate has increased; (3) Perturbations from other planets affected the evolution (Ćuk, 2007); or (4) Linear theory is oversimplified. Probably all these possibilities play a role and make the extension of tidal theory to an Earth-like exoplanet unreliable. Measurements of the martian dissipation function find $Q_{\rm Mars} = 85.58 \pm 0.37$ (Bills *et al.,* 2005) or $Q_{\rm Mars} = 79.91 \pm 0.69$ (Lainey *et al.,* 2007). The value for Mercury is $Q_{\rm Mercury} < 190$, and for Venus it is $Q_{\rm Venus} < 17$ (Goldreich and Soter, 1966). Observations of Io imply $Q_{\rm Io} < 100$ (Peale *et al.,* 1979; Segatz *et al.,* 1988), while the Moon lies at $Q_{\rm Moon} = 26.5 \pm 1$ (Dickey *et al.,* 1994). These measurements indicate a similar order of magnitude for the tidal dissipation function of all desiccated bodies in the Solar System.

Tidal effects on Venus may be particularly complicated due to its large atmosphere. The rotation rate of Venus is such that it always presents the same face to Earth at inferior conjunction. Although this may be by chance due to Venus approaching tidal lock with the Sun, it has also been suggested that at some point in the past thermal atmospheric tides could have provided an equal but opposite torque than that from the rocky component. If that occurred, the torque from Earth could dominate and spin-lock Venus to the Earth (Gold and Soter, 1969). More recent and detailed work has shown that this interaction can be significant and permits chaotic spin evolution that eventually settles into one of four possible states (Correia and Laskar, 2001). Although a large atmosphere can play a significant role in the evolution of terrestrial planets (Correia and Laskar, 2003), we ignore their effect here due to the large number of unknowns for an exoplanet. In real bodies, Q is a function of the bodies' rigidity μ, viscosity η, and temperature T (Segatz *et al.,* 1988; Fischer and Spohn, 1990). A comprehensive tidal model would couple the orbital and structural evolution of the bodies since small perturbations in T can result in large variations in Q (Segatz *et al.,* 1988; Mardling and Lin, 2002; Efroimsky and Lainey, 2007). Moreover, tidally generated heat will not necessarily be transported to the surface quickly. The internal structure of the planet may trap the energy for long periods of time, resulting in catastrophic tectonics when the heat is finally released, as may have occurred on Venus (Turcotte, 1996). This episodic volcanism could change $t_{\rm des}$ dramatically, but on the other hand, complete lithospheric overturn is probably just as detrimental to life as desiccation. Nonetheless, future work should explore these details. Henning *et al.* (2009) performed detailed calculations and argued that $k_2 = 0.3$ and $Q = 50$ are reasonable choices for dry planets.

The tidal properties of stars are about as poorly constrained as they are for planets. The primary constraint comes from the distribution of orbits of binary stars (*e.g.,* Zahn, 1977), whose orbits are circularized by the tidal interaction. However, for the closest binaries, where the tidal effects are strongest and one might think the constraints the tightest, the situation is complicated by the early phases of stellar evolution (Zahn and Bouchet, 1989), in which stellar radii contract rapidly. As the radius enters the tidal evolution at the $5^{\rm th}$ power, the radial contraction is a major effect. Khaliullin and Khaliullina (2011) revisited this point and found that, although radial contraction does play a major role, they were unable to combine models of the equilibrium tide and radial contraction to match observations. Weinberg *et al.* (2011) tested the linear theory against nonlinear models and found that in general the linear theory does not capture the physics of the more sophisticated approach. These studies demonstrate that there still exist serious problems with the linear theory, and quantitative discrepancies exist. However, it does qualitatively model the relevant physics and allows wide sweeps of parameter space to be a computationally tractable problem. We therefore continue to use it but explicitly acknowledge that known weaknesses persist.

A wide range of values for the tidal quality factor and tidal time lag for stars is present in the literature, ranging from $Q_* = 10^4$ (Adams *et al.,* 2011) all the way to $Q_* = 10^9$ (Matsumura *et al.,* 2010), with many others finding intermediate values (*e.g.,* Lin *et al.,* 1996; Carone and Pätzold, 2007; Jackson *et al.,* 2008b, 2009; Ibgui and Burrows, 2009). For the star, we take an intermediate and typical value of $Q_* = 10^6$.

Acknowledgments

This work was funded by NASA Astrobiology Institute's Virtual Planetary Laboratory lead team, under cooperative

agreement No. NNH05ZDA001C. R.B. acknowledges additional funding from NSF grant AST-1108882. We are also grateful for stimulating discussions with Richard Greenberg, Norm Sleep, Sean Raymond, and Andrew Rushby.

Abbreviations

CPL, constant phase lag; CTL, constant time lag; HZ, habitable zone; IHZ, insolation habitable zone; XUV, extreme ultraviolet.

B98, Baraffe *et al.* (1998); BO06, Bayless and Orosz (2006); GS99, Gorda and Svechnikov (1999); RH00, Reid and Hawley (2000); S07, Scalo *et al.* (2007).

References

Abe, Y. and Matsui, T. (1988) Evolution of an impact generated H_2O–CO_2 atmosphere and formation of a hot proto-ocean on Earth. *Journal of Atmospheric Sciences* 45:3081–3101.

Abe, Y., Abe-Ouchi, A., Sleep, N.H., and Zahnle, K.J. (2011) Habitable zone limits for dry planets. *Astrobiology* 11:443–460.

Adams, E.R., López-Morales, M., Elliot, J.L., Seager, S., and Osip D.J. (2011) Transit timing variation analysis of OGLE-TR-132b with seven new transits. *Astrophys J* 728, doi:10.1088/0004-637X/728/2/125.

Agol, E. (2011) Transit surveys for Earths in the habitable zones of white dwarfs. *Astrophys J* 731:L31.

Aksnes, K. and Franklin, F.A. (2001) Secular acceleration of Io derived from mutual satellite events. *Astron J* 122:2734–2739.

Anglada-Escudé, G., Arriagada, P., Vogt, S.S., Rivera, E.J., Butler, R.P., Crane, J.D., Shectman, S.A., Thompson, I.B., Minniti, D., Haghighipour, N., Carter, B.D., Tinney, C.G., Wittenmyer, R.A., Bailey, J.A., O'Toole, S.J., Jones, H.R.A., and Jenkins J.S. (2012) A planetary system around the nearby M dwarf GJ 667C with at least one super-Earth in its habitable zone. arXiv:1202.0446.

Baraffe, I., Chabrier, G., Allard, F., and Hauschildt, P.H. (1998) Evolutionary models for solar metallicity low-mass stars: mass-magnitude relationships and color-magnitude diagrams. *Astron Astrophys* 337:403–412.

Barnes, R., Raymond, S.N., Jackson, B., and Greenberg, R. (2008) Tides and the evolution of planetary habitability. *Astrobiology* 8:557–568.

Barnes, R., Jackson, B., Greenberg, R., and Raymond, S.N. (2009a) Tidal limits to planetary habitability. *Astrophys J* 700:L30–L33.

Barnes, R., Jackson, B., Raymond, S.N., West, A.A., and Greenberg, R. (2009b) The HD 40307 planetary system: super-Earths or mini-Neptunes? *Astrophys J* 695, doi:10.1088/0004-637X/695/2/1006.

Barnes, R., Raymond, S.N., Greenberg, R., Jackson, B., and Kaib, N.A. (2010) CoRoT-7b: super-Earth or super-Io? *Astrophys J* 709:L95–L98.

Batalha, N.M., Borucki, W.J., Bryson, S.T., Buchhave, L.A., Caldwell, D.A., Christensen-Dalsgaard, J., Ciardi, D., Dunham, E.W., Fressin, F., Gautier, T.N., III, Gilliland, R.L., Haas, M.R., Howell, S.B., Jenkins, J.M., Kjeldsen, H., Koch, D.G., Latham, D.W., Lissauer, J.J., Marcy, G.W., Rowe, J.F., Sasselov, D.D., Seager, S., Steffen, J.H., Torres, G., Basri, G.S., Brown, T.M., Charbonneau, D., Christiansen, J., Clarke, B., Cochran, W.D., Dupree, A., Fabrycky, D.C., Fischer, D., Ford, E.B., Fortney, J., Girouard, F.R., Holman, M.J., Johnson, J., Isaacson, H., Klaus, T.C., Machalek, P., Moorehead, A.V., Morehead, R.C., Ragozzine, D., Tenenbaum, P., Twicken, J., Quinn, S., VanCleve, J., Walkowicz, L.M., Welsh, W.F., Devore, E., and Gould, A. (2011) Kepler's first rocky planet: Kepler-10b. *Astrophys J* 729, doi:10.1088/0004-637X/729/1/27.

Bayless, A.J. and Orosz, J.A. (2006) 2MASS J05162881+2607387: a new low-mass double-lined eclipsing binary. *Astrophys J* 651:1155–1165.

Bean, J.L., Seifahrt, A., Hartman, H., Nilsson, H., Wiedemann, G., Reiners, A., Dreizler, S., and Henry, T.J. (2010) The CRIRES search for planets around the lowest-mass stars. I. High-precision near-infrared radial velocities with an ammonia gas cell. *Astrophys J* 713:410–422.

Běhounková, M., Tobie, G., Choblet, G., and Čadek, O. (2011) Tidally induced thermal runaways on extrasolar Earths: impact on habitability. *Astrophys J* 728, doi:10.1088/0004-637X/728/2/89.

Bell, D.R. and Rossman, G.R. (1992) Water in Earth's mantle—the role of nominally anhydrous minerals. *Science* 255:1391–1397.

Bills, B.G., Neumann, G.A., Smith, D.E., and Zuber M.T. (2005) Improved estimate of tidal dissipation within Mars from MOLA observations of the shadow of Phobos. *J Geophys Res* 110:E07004.

Blaney, D.L., Johnson, T.V., Matson, D.L., and Veeder, G.J. (1995) Volcanic eruptions on Io: heat flow, resurfacing, and lava composition. *Icarus* 113:220–225.

Bolmont, E., Raymond, S.N., and Leconte, J. (2011) Tidal evolution of planets around brown dwarfs. arXiv:1109.2906.

Bond, J.C., O'Brien, D.P., and Lauretta, D.S. (2010) The compositional diversity of extrasolar terrestrial planets. I. *In situ* simulations. *Astrophys J* 715, doi:10.1088/0004-637X/715/2/1050.

Bonfils, X., Delfosse, X., Udry, S., Forveille, T., Mayor, M., Perrier, C., Bouchy, F., Gillon, M., Lovis, C., Pepe, F., Queloz, D., Santos, N.C., Ségransan, D., and Bertaux J.-L. (2011) The HARPS search for southern extra-solar planets XXXI. The M-dwarf sample. arXiv:1111.5019.

Boss, A.P., Weinberger, A.J., Anglada-Escudé, G., Thompson, I.B., Burley, G., Birk, C., Pravdo, S.H., Shaklan, S.B., Gatewood, G.D., Majewski, S.R., and Patterson, R.J. (2009) The Carnegie Astrometric Planet Search Program. *Publ Astron Soc Pac* 121:1218–1231.

Butler, R.P., Wright, J.T., Marcy, G.W., Fischer, D.A., Vogt, S.S., Tinney, C.G., Jones, H.R.A., Carter, B.D., Johnson, J.A., McCarthy, C., and Penny, A.J. (2006) Catalog of nearby exoplanets. *Astrophys J* 646:505–522.

Carone, L. and Pätzold, M. (2007) Constraints on the tidal dissipation factor of a main sequence star: the case of OGLE-TR-56b. *Planet Space Sci* 55:643–650.

Carter, J.A. Winn, J.N., Holman, M.J., Fabrycky, D., Berta, Z.K., Burke, C.J., and Nutzman, P. (2011) The Transit Light Curve Project. XIII. Sixteen transits of the super-Earth GJ 1214b. *Astrophys J* 730, doi:10.1088/0004-637X/730/2/82.

Charbonneau, D., Berta, Z.K., Irwin, J., Burke, C.J., Nutzman, P., Buchhave, L.A., Lovis, C., Bonfils, X., Latham, D.W., Udry, S., Murray-Clay, R.A., Holman, M.J., Falco, E.E., Winn, J.N., Queloz, D., Pepe, F., Mayor, M., Delfosse, X., and Forveille, T. (2009) A super-Earth transiting a nearby low-mass star. *Nature* 462:891–894.

Chassefière, E. (1996) Hydrodynamic escape of hydrogen from a hot water-rich atmosphere: the case of Venus. *J Geophys Res* 101, doi:10.1029/96JE01951.

Correia, A.C.M. and Laskar J. (2001) The four final rotation states of Venus. *Nature* 411:767–770.

Correia, A.C.M. and Laskar, J. (2003) Different tidal torques on a planet with a dense atmosphere and consequences to the spin dynamics. *J Geophys Res* 108:5123.

Correia, A.C.M., Levrard, B., and Laskar, J. (2008) On the equilibrium rotation of Earth-like extra-solar planets. *Astron Astrophys* 488:L63–L66.

Ćuk, M. (2007) Excitation of lunar eccentricity by planetary resonances. *Science* 318:244.

Cushing, M.C., Kirkpatrick, J.D., Gelino, C.R., Griffith, R.L., Skrutskie, M.F., Mainzer, A.K., Marsh, K.A., Beichman, C.A., Burgasser, A.J., Prato, L.A., Simcoe, R.A., Marley, M.S., Saumon, D., Freedman, R.S., Eisenhardt, P.R., and Wright, E.L. (2011) The discovery of Y dwarfs using data from the Wide-field Infrared Survey Explorer (WISE). arXiv:1108.4678.

Darwin, G.H. (1880) On the secular changes in the elements of the orbit of a satellite revolving about a tidally distorted planet. *Royal Society of London Philosophical Transactions Series I* 171:713–891.

Dawson, R.I. and Fabrycky, D.C. (2010) Radial velocity planets de-aliased: a new, short period for super-Earth 55 Cnc e. *Astrophys J* 722:937–953.

de Bergh, C. (1993) The D/H ratio and the evolution of water in the terrestrial planets. *Orig Life Evol Biopsh* 23:11–21.

Delfosse, X., Bonfils, X., Forveille, T., Udry, S., Mayor, M., Bouchy, F., Gillon, M., Lovis, C., Neves, V., Pepe, F., Perrier, C., Queloz, D., Santos, N.C., and Ségransan, D. (2012) The HARPS search for southern extra-solar planets XXXV. Super-Earths around the M-dwarf neighbors Gl433 and Gl667C. arXiv:1202.2467.

Dickey, J.O., Bender, P.L., Faller, J.E., Newhall, X.X., Ricklefs, R.L., Ries, J.G., Shelus, P.J., Veillet, C., Whipple, A.L., Wiant, J.R., Williams, J.G., and Yoder, C.F. (1994) Lunar Laser Ranging: a continuing legacy of the Apollo program. *Science* 265:482–490.

Dole, S.H. (1964) *Habitable Planets for Man,* Blaisdell, New York.

Donahue, T.M., Hoffman, J.H., Hodges, R.R., and Watson, A.J. (1982) Venus was wet—a measurement of the ratio of deuterium to hydrogen. *Science* 216:630–633.

Driscoll, P. and Olson, P. (2011) Optimal dynamos in the cores of terrestrial exoplanets: magnetic field generation and detectability. *Icarus* 213:12–23.

Edson, A., Lee, S., Bannon, P., Kasting, J.F., and Pollard, D. (2011) Atmospheric circulations of terrestrial planets orbiting low-mass stars. *Icarus* 212:1–13.

Efroimsky, M. and Lainey, V. (2007) Physics of bodily tides in terrestrial planets and the appropriate scales of dynamical evolution. *J Geophys Res* 112:E12003.

Efroimsky, M. and Williams, J.G. (2009) Tidal torques: a critical review of some techniques. *Celestial Mechanics and Dynamical Astronomy* 104:257–289.

Egbert, G.D. and Ray, R.D. (2000) Significant dissipation of tidal energy in the deep ocean inferred from satellite altimeter data. *Nature* 405:775–778.

Erkaev, N.V., Kulikov, Y.N., Lammer, H., Selsis, F., Langmayr, D., Jaritz, G.F., and Biernat, H.K. (2007) Roche lobe effects on the atmospheric loss from "hot Jupiters." *Astron Astrophys* 472:329–334.

Ferraz-Mello, S., Rodríguez, A., and Hussmann, H. (2008) Tidal friction in close-in satellites and exoplanets: the Darwin theory re-visited. *Celestial Mechanics and Dynamical Astronomy* 101:171–201.

Fischer, H.-J. and Spohn, T. (1990) Thermal-orbital histories of viscoelastic models of Io (J1). *Icarus* 83:39–65.

Fleming, T.A., Giampapa, M.S., Schmitt, J.H.M.M., and Bookbinder, J.A. (1993) Stellar coronae at the end of the main sequence—a ROSAT survey of the late M dwarfs. *Astrophys J* 410:387–392.

Fontaine, F.J., Olive, J.-A., Cannat, M., Escartin, J., and Perol, T. (2011) Hydrothermally induced melt lens cooling and segmentation along the axis of fast- and intermediate-spreading centers. *Geophys Res Lett* 381:L14307.

Fortney, J.J., Marley, M.S., and Barnes, J.W. (2007) Planetary radii across five orders of magnitude in mass and stellar insolation: application to transits. *Astrophys J* 659:1661–1672.

Forveille, T., Bonfils, X., Delfosse, X., Alonso, R., Udry, S., Bouchy, F., Gillon, M., Lovis, C., Neves, V., Mayor, M., Pepe, F., Queloz, D., Santos, N.C., Segransan, D., Almenara, J.M., Deeg, H., and Rabus, M. (2011) The HARPS search for southern extra-solar planets XXXII. Only 4 planets in the Gl ~ 581 system. arXiv:1109.2505.

Garrett, C. and Kunze, E. (2007) Internal tide generation in the deep ocean. *Annu Rev Fluid Mech* 39:57–87.

Gold, T. and Soter, S. (1969) Atmospheric tides and the resonant rotation of Venus. *Icarus* 11:356–366.

Goldblatt, C. and Watson, A.J. (2012) The runaway greenhouse: implications for future climate change, geoengineering and planetary atmospheres. arXiv:1201.1593.

Goldreich, P. (1966) Final spin states of planets and satellites. *Astron J* 71:1–7.

Goldreich, P. and Soter, S. (1966) *Q* in the Solar System. *Icarus* 5:375–389.

Gorda, S.Y. and Svechnikov, M.A. (1999) Empirical *L-M, R-M,* and M-$T_{\rm eff}$ relations for main-sequence stars: components of close binary systems and low-mass stars. *Astronomy Reports* 43:521–525.

Grasset, O., Schneider, J., and Sotin, C. (2009) A study of the accuracy of mass-radius relationships for silicate-rich and ice-rich planets up to 100 Earth masses. *Astrophys J* 693:722–733.

Greenberg, R. (2009) Frequency dependence of tidal *q*. *Astrophys J* 698:L42–L45.

Greenberg, R. and Weidenschilling, S.J. (1984) How fast do Galilean satellites spin? *Icarus* 58:186–196.

Hansen, C.J., Esposito, L., Stewart, A.I.F., Colwell, J., Hendrix, A., Pryor, W., Shemansky, D., and West, R. (2006) Enceladus' water vapor plume. *Science* 311:1422–1425.

Hart, M.H. (1979) Habitable zones about main sequence stars. *Icarus* 37:351–357.

Hawley, S.L. and Pettersen, B.R. (1991) The great flare of 1985 April 12 on AD Leonis. *Astrophys J* 378:725–741.

Heller, R., Leconte, J., and Barnes, R. (2011) Tidal obliquity evolution of potentially habitable planets. *Astron Astrophys* 528:A27.

Heng, K. and Vogt, S.S. (2011) Gliese 581g as a scaled-up version of Earth: atmospheric circulation simulations. *Mon Not R Astron Soc* 415:2145–2157.

Henning, W.G., O'Connell, R.J., and Sasselov, D.D. (2009) Tidally heated terrestrial exoplanets: viscoelastic response models. *Astrophys J* 707:1000–1015.

Holden, J.F., Summit, M., and Baross J.A. (1998) Thermophilic and hyperthermophilic microorganisms in 3–30°C hydrothermal fluids following a deep-sea volcanic eruption. *FEMS Microbiol Ecol* 25:33–41.

Hurford, T.A., Helfenstein, P., Hoppa, G.V., Greenberg, R., and Bills, B.G. (2007) Eruptions arising from tidally controlled periodic openings of rifts on Enceladus. *Nature* 447:292–294.

Hut, P. (1981) Tidal evolution in close binary systems. *Astron Astrophys* 99:126–140.

Ibgui, L. and Burrows, A. (2009) Coupled evolution with tides of the radius and orbit of transiting giant planets: general results. *Astrophys J* 700:1921–1932.

Ingersoll, A.P. (1969) The runaway greenhouse: a history of water on Venus. *Journal of the Atmospheric Sciences* 26:1191–1198.

Jackson, B., Barnes, R., and Greenberg, R. (2008a) Tidal heating of terrestrial extrasolar planets and implications for their habitability. *Mon Not R Astron Soc* 391:237–245.

Jackson, B., Greenberg, R., and Barnes, R. (2008b) Tidal evolution of close-in extrasolar planets. *Astrophys J* 678:1396–1406.

Jackson, B., Greenberg, R., and Barnes, R. (2008c) Tidal heating of extrasolar planets. *Astrophys J* 681:1631–1638.

Jackson, B., Barnes, R., and Greenberg, R. (2009) Observational evidence for tidal destruction of exoplanets. *Astrophys J* 698:1357–1366.

Jackson, B., Miller, N., Barnes, R., Raymond, S.N., Fortney, J.J., and Greenberg, R. (2010) The roles of tidal evolution and evaporative mass loss in the origin of CoRoT-7 b. *Mon Not R Astron Soc* 407:910–922.

Jayne, S.R. (2001) Parameterizing tidal dissipation over rough topography. *Geophys Res Lett* 28:811–814.

Johnson, T.V., Cook, A.F., II, Sagan, C., and Soderblom, L.A. (1979) Volcanic resurfacing rates and implications for volatiles on Io. *Nature* 280:746–750.

Jones, H.R.A., Butler, R.P., Tinney, C.G., Marcy, G.W., Carter, B.D., Penny, A.J., McCarthy, C., and Bailey, J. (2006) High-eccentricity planets from the Anglo-Australian Planet Search. *Mon Not R Astron Soc* 369:249–256.

Joshi, M. (2003) Climate model studies of synchronously rotating planets. *Astrobiology* 3:415–427.

Joshi, M.M., Haberle, R.M., and Reynolds, R.T. (1997) Simulations of the atmospheres of synchronously rotating terrestrial planets orbiting M dwarfs: conditions for atmospheric collapse and the implications for habitability. *Icarus* 129:450–465.

Kaltenegger, L. and Traub, W.A. (2009) Transits of Earth-like planets. *Astrophys J* 698:519–527.

Kasting, J.F. (1988) Runaway and moist greenhouse atmospheres and the evolution of Earth and Venus. *Icarus* 74:472–494.

Kasting, J.F. and Pollack, J.B. (1983) Loss of water from Venus. I—Hydrodynamic escape of hydrogen. *Icarus* 53:479–508.

Kasting, J.F., Whitmire, D.P., and Reynolds, R.T. (1993) Habitable zones around main sequence stars. *Icarus* 101:108–128.

Kelly, S.M., Nash, J.D., and Kunze, E. (2010) Internal-tide energy over topography. *J Geophys Res* 115:C06014.

Khaliullin, K.F. and Khaliullina, A.I. (2011) Orbital circularization of close binary stars on the pre-main sequence. *Mon Not R Astron Soc* 411:2804–2816.

Khodachenko, M.L., Ribas, I., Lammer, H., Grießmeier, J.-M., Leitner, M., Selsis, F., Eiroa, C., Hanslmeier, A., Biernat, H.K., Farrugia, C.J., and Rucker, H.O. (2007) Coronal mass ejection (CME) activity of low-mass M stars as an important factor for the habitability of terrestrial exoplanets. I. CME impact on expected magnetospheres of Earth-like exoplanets in close-in habitable zones. *Astrobiology* 7:167–184.

Kokubo, E. and Ida, S. (1998) Oligarchic growth of protoplanets. *Icarus* 131:171–178.

Komabayashi, M. (1967) Discrete equilibrium temperatures of a hypothetical planet with the atmosphere and the hydrosphere of a one component–two phase system under constant solar radiation. *Journal of the Meteorological Society of Japan* 45:137–139.

Koriski, S. and Zucker, S. (2011) On the ages of planetary systems with mean-motion resonances. *Astrophys J* 741:L23.

Kowalski, A.F., Hawley, S.L., Holtzman, J.A., Wisniewski, J.P., and Hilton, E.J. (2012) The multiple continuum components in the white-light flare of 16 January 2009 on the dM4.5e Star YZ CMi. *Solar Physics* 277:21–29.

Kundurthy, P., Agol, E., Becker, A.C., Barnes, R., Williams, B., and Mukadam, A. (2011) APOSTLE observations of GJ 1214b: system parameters and evidence for stellar activity. *Astrophys J* 731, doi:10.1088/0004-637X/731/2/123.

Lainey, V., Dehant, V., and Pätzold, M. (2007) First numerical ephemerides of the martian moons. *Astron Astrophys* 465:1075–1084.

Lainey, V., Arlot, J.-E., Karatekin, Ö., and van Hoolst, T. (2009) Strong tidal dissipation in Io and Jupiter from astrometric observations. *Nature* 459:957–959.

Lambeck, K. (1977) Tidal dissipation in the oceans: astronomical, geophysical and oceanographic consequences. *Philos Transact A Math Phys Eng Sci* 287:545–594.

Lammer, H., Lichtenegger, H.I.M., Kulikov, Y.N., Grießmeier, J.-M., Terada, N., Erkaev, N.V., Biernat, H.K., Khodachenko, M.L., Ribas, I., Penz, T., and Selsis, F. (2007) Coronal mass ejection (CME) activity of low-mass M stars as an important factor for the habitability of terrestrial exoplanets. II. CME-induced ion pick up of Earth-like exoplanets in close-in habitable zones. *Astrobiology* 7:185–207.

Lammer, H., Odert, P., Leitzinger, M., Khodachenko, M.L., Panchenko, M., Kulikov, Y.N., Zhang, T.L., Lichtenegger, H.I.M., Erkaev, N.V., Wuchterl, G., Micela, G., Penz, T., Biernat, H.K., Weingrill, J., Steller, M., Ottacher, H., Hasiba, J., and Hanslmeier, A. (2009) Determining the mass loss limit for close-in exoplanets: what can we learn from transit observations? *Astron Astrophys* 506:399–410.

Lammer, H., Selsis, F., Chassefière, E., Breuer, D., Grießmeier, J.-M., Kulikov, Y.N., Erkaev, N.V., Khodachenko, M.L., Biernat, H.K., Leblanc, F., Kallio, E., Lundin, R., Westall, F., Bauer, S.J., Beichman, C., Danchi, W., Eiroa, C., Fridlund, M., Gröller, H., Hanslmeier, A., Hausleitner, W., Henning, T., Herbst, T., Kaltenegger, L., Léger, A., Leitzinger, M., Lichtenegger, H.I.M., Liseau, R., Lunine, J., Motschmann, U., Odert, P., Paresce, F., Parnell, J., Penny, A., Quirrenbach, A., Rauer, H., Röttgering, H., Schneider, J., Spohn, T., Stadelmann, A., Stangl, G., Stam, D., Tinetti, G., and White, G.J. (2010) Geophysical and atmospheric evolution of habitable planets. *Astrobiology* 10:45–68.

Laver, C., de Pater, I., and Marchis, F. (2007) Tvashtar awakening detected in April 2006 with OSIRIS at the W.M. Keck Observatory. *Icarus* 191:749–754.

Lecar, M. and Aarseth, S.J. (1986) A numerical simulation of the formation of the terrestrial planets. *Astrophys J* 305:564–579.

Leconte, J., Chabrier, G., Baraffe, I., and Levrard, B. (2010) Is tidal heating sufficient to explain bloated exoplanets? Consistent calculations accounting for finite initial eccentricity. *Astron Astrophys* 516:A64.

Léger, A., Selsis, F., Sotin, C., Guillot, T., Despois, D., Mawet, D., Ollivier, M., Labèque, A., Valette, C., Brachet, F., Chazelas, B., and Lammer, H. (2004) A new family of planets? "Ocean-Planets." *Icarus* 169:499–504.

Léger, A., Rouan, D., Schneider, J., Barge, P., Fridlund, M., Samuel, B., Ollivier, M., Guenther, E., Deleuil, M., Deeg, H.J., Auvergne, M., Alonso, R., Aigrain, S., Alapini, A., Almenara, J.M., Baglin, A., Barbieri, M., Bruntt, H., Bordé, P., Bouchy, F., Cabrera, J., Catala, C., Carone, L., Carpano, S., Csizmadia, S., Dvorak, R., Erikson, A., Ferraz-Mello, S., Foing, B., Fressin, F., Gandolfi, D., Gillon, M., Gondoin, P., Grasset, O., Guillot, T., Hatzes, A., Hébrard, G., Jorda, L., Lammer, H., Llebaria, A.,

Loeillet, B., Mayor, M., Mazeh, T., Moutou, C., Pätzold, M., Pont, F., Queloz, D., Rauer, H., Renner, S., Samadi, R., Shporer, A., Sotin, C., Tingley, B., Wuchterl, G., Adda, M., Agogu, P., Appourchaux, T., Ballans, H., Baron, P., Beaufort, T., Bellenger, R., Berlin, R., Bernardi, P., Blouin, D., Baudin, F., Bodin, P., Boisnard, L., Boit, L., Bonneau, F., Borzeix, S., Briet, R., Buey, J.-T., Butler, B., Cailleau, D., Cautain, R., Chabaud, P.-Y., Chaintreuil, S., Chiavassa, F., Costes, V., Cuna Parrho, V., de Oliveira Fialho, F., Decaudin, M., Defise, J.-M., Djalal, S., Epstein, G., Exil, G.-E., Fauré, C., Fenouillet, T., Gaboriaud, A., Gallic, A., Gamet, P., Gavalda, P., Grolleau, E., Gruneisen, R., Gueguen, L., Guis, V., Guivarc'h, V., Guterman, P., Hallouard, D., Hasiba, J., Heuripeau, F., Huntzinger, G., Hustaix, H., Imad, C., Imbert, C., Johlander, B., Jouret, M., Journoud, P., Karioty, F., Kerjean, L., Lafaille, V., Lafond, L., Lam-Trong, T., Landiech, P., Lapeyrere, V., Larqué, T., Laudet, P., Lautier, N., Lecann, H., Lefevre, L., Leruyet, B., Levacher, P., Magnan, A., Mazy, E., Mertens, F., Mesnager, J.-M., Meunier, J.-C., Michel, J.-P., Monjoin, W., Naudet, D., Nguyen-Kim, K., Orcesi, J.-L., Ottacher, H., Perez, R., Peter, G., Plasson, P., Plesseria, J.-Y., Pontet, B., Pradines, A., Quentin, C., Reynaud, J.-L., Rolland, G., Rollenhagen, F., Romagnan, R., Russ, N., Schmidt, R., Schwartz, N., Sebbag, I., Sedes, G., Smit, H., Steller, M.B., Sunter, W., Surace, C., Tello, M., Tiphène, D., Toulouse, P., Ulmer, B., Vandermarcq, O., Vergnault, E., Vuillemin, A., and Zanatta, P. (2009) Transiting exoplanets from the CoRoT space mission. VIII. CoRoT-7b: the first super-Earth with measured radius. *Astron Astrophys* 506:287–302.

Levrard, B., Winisdoerffer, C., and Chabrier, G. (2009) Falling transiting extrasolar giant planets. *Astrophys J* 692:L9–L13.

Lin, D.N.C., Bodenheimer, P., and Richardson, D.C. (1996) Orbital migration of the planetary companion of 51 Pegasi to its present location. *Nature* 380:606–607.

Lissauer, J.J. (1993) Planet formation. *Annu Rev Astron Astrophys* 31:129–174.

Lissauer, J.J. (2007) Planets formed in habitable zones of M dwarf stars probably are deficient in volatiles. *Astrophys J* 660:L149–L152.

Lunine, J.I., Fischer, D., Hammel, H.B., Henning, T., Hillenbrand, L., Kasting, J., Laughlin, G., Macintosh, B., Marley, M., Melnick, G., Monet, D., Noecker, C., Peale, S., Quirrenbach, A., Seager, S., and Winn, J.N. (2008) Worlds beyond: a strategy for the detection and characterization of exoplanets. Executive summary of a report of the ExoPlanet Task Force Astronomy and Astrophysics Advisory Committee Washington, DC, June 23, 2008. *Astrobiology* 8:875–881.

MacDonald, G.J.F. (1964) Tidal friction. *Reviews of Geophysics and Space Physics* 2:467–541.

Makarov, V.V. and Efroimsky, M. (2012) No pseudosynchronous rotation for terrestrial planets and moons. arXiv: 1209.1616.

Mandell, A.M., Raymond, S.N., and Sigurdsson, S. (2007) Formation of Earth-like planets during and after giant planet migration. *Astrophys J* 660:823–844.

Mardling, R.A. and Lin, D.N.C. (2002) Calculating the tidal, spin, and dynamical evolution of extrasolar planetary systems. *Astrophys J* 573:829–844.

Marty, B. and Yokochim, R. (2006) Water in the early Earth. *Reviews in Mineralogy and Geochemistry* 62:421–450.

Matsumura, S., Peale, S.J., and Rasio, F.A. (2010) Tidal evolution of close-in planets. *Astrophys J* 725:1995–2016.

Mayor, M., Bonfils, X., Forveille, T., Delfosse, X., Udry, S., Bertaux, J.-L., Beust, H., Bouchy, F., Lovis, C., Pepe, F., Perrier, C., Queloz, D., and Santos, N.C. (2009) The HARPS search for southern extra-solar planets. XVIII. An Earth-mass planet in the GJ 581 planetary system. *Astron Astrophys* 507:487–494.

McArthur, B.E., Endl, M., Cochran, W.D., Benedict, G.F., Fischer, D.A., Marcy, G.W., Butler, R.P., Naef, D., Mayor, M., Queloz, D., Udry, S., and Harrison T.E. (2004) Detection of a Neptune-mass planet in the ρ^1 Cancri system using the Hobby-Eberly telescope. *Astrophys J* 614:L81–L84.

McEwen, A.S., Keszthelyi, L.P., Lopes, R., Schenk, P.M., and Spencer, J.R. (2004) The lithosphere and surface of Io. In *Jupiter: The Planet, Satellites and Magnetosphere,* edited by F. Bagenal, T.E. Dowling, and W.B. McKinnon, Cambridge University Press, Cambridge, UK, pp 307–328.

Monteiro, H. (2010) The habitable zones of white dwarfs. *Bulletin of the Astronomical Society of Brazil* 29:22–25.

Murakami, M., Hirose, K., Yurimoto, H., Nakashima, S., and Takafuji, N. (2002) Water in Earth's lower mantle. *Science* 295:1885–1887.

Murray, C.D. and Dermott, S.F. (1999) *Solar System Dynamics,* Cambridge University Press, Cambridge, UK.

Naef, D., Latham, D.W., Mayor, M., Mazeh, T., Beuzit, J.L., Drukier, G.A., Perrier-Bellet, C., Queloz, D., Sivan, J.P., Torres, G., Udry, S., and Zucker, S. (2001) HD 80606 b, a planet on an extremely elongated orbit. *Astron Astrophys* 375:L27–L30.

Nakajima, S., Hayashi, Y.-Y., and Abe, Y. (1992) A study of the "runaway greenhouse effect" with a one-dimensional radiative convective model. *Journal of the Atmospheric Sciences* 49:2256–2266.

Neron de Surgy, O. and Laskar, J. (1997) On the long term evolution of the spin of the Earth. *Astron Astrophys* 318:975–989.

Nesvorný, D. (2011) Young solar system's fifth giant planet? *Astrophys J* 742:L22.

Nutzman, P. and Charbonneau, D. (2008) Design considerations for a ground-based transit search for habitable planets orbiting M dwarfs. *Publ Astron Soc Pac* 120:317–327.

Nycander, J. (2005) Generation of internal waves in the deep ocean by tides. *J Geophys Res* 110:C10028.

O'Brien, D.P., Morbidelli, A., and Levison, H.F. (2006) Terrestrial planet formation with strong dynamical friction. *Icarus* 184:39–58.

Olson, P. and Christensen, U.R. (2006) Dipole moment scaling for convection-driven planetary dynamos. *Earth Planet Sci Lett* 250:561–571.

Peale, S.J., Cassen, P., and Reynolds, R.T. (1979) Melting of Io by tidal dissipation. *Science* 203:892–894.

Pierrehumbert, R.T. (2010) *Principles of Planetary Climate,* Cambridge University Press, Cambridge, UK.

Pierrehumbert, R.T. (2011) A palette of climates for Gliese 581g. *Astrophys J* 726:L8.

Pollack, J.B. (1971) A nongrey calculation of the runaway greenhouse: implications for Venus' past and present. *Icarus* 14:295–306.

Porco, C.C., Helfenstein, P., Thomas, P.C., Ingersoll, A.P., Wisdom, J., West, R., Neukum, G., Denk, T., Wagner, R., Roatsch, T., Kieffer, S., Turtle, E., McEwen, A., Johnson, T.V., Rathbun, J., Veverka, J., Wilson, D., Perry, J., Spitale, J., Brahic, A., Burns, J.A., Del Genio, A.D., Dones, L., Murray, C.D., and Squyres, S. (2006) Cassini observes the active south pole of Enceladus. *Science* 311:1393–1401.

Raymond, S.N., Quinn, T., and Lunine, J.I. (2004) Making other earths: dynamical simulations of terrestrial planet formation and water delivery. *Icarus* 168:1–17.

Raymond, S.N., Mandell, A.M., and Sigurdsson, S. (2006) Exotic earths: forming habitable worlds with giant planet migration. *Science* 313:1413–1416.

Raymond, S.N., Scalo, J., and Meadows, V.S. (2007) A decreased probability of habitable planet formation around low-mass stars. *Astrophys J* 669:606–614.

Reid, I.N. and Hawley, S.L. (2000) *New Light on Dark Stars: Red Dwarfs, Low-Mass Stars, Brown Dwarfs,* Springer, New York.

Ribas, I., Guinan, E.F., Güdel, M., and Audard, M. (2005) Evolution of the solar activity over time and effects on planetary atmospheres. I. High-energy irradiances (1–1700 Å). *Astrophys J* 622, doi:10.1086/427977.

Rodler, F., Del Burgo, C., Witte, S., Helling, C., Hauschildt, P.H., Martín, E.L., Álvarez, C., and Deshpande, R. (2011) Detecting planets around very cool dwarfs at near infrared wavelengths with the radial velocity technique. *Astron Astrophys* 532:A31.

Rodríguez, A., Callegari, N., Jr., Michtchenko, T.A., and Hussmann, H. (2012) Spin-orbit coupling for tidally evolving super-Earths. arXiv:1209.1580.

Sada, P.V., Deming, D., Jackson, B., Jennings, D.E., Peterson, S.W., Haase, F., Bays, K., O'Gorman, E., and Lundsford, A. (2010) Recent transits of the super-Earth exoplanet GJ 1214b. *Astrophys J* 720:L215–L218.

Scalo, J., Kaltenegger, L., Segura, A.G., Fridlund, M., Ribas, I., Kulikov, Y.N., Grenfell, J.L., Rauer, H., Odert, P., Leitzinger, M., Selsis, F., Khodachenko, M.L., Eiroa, C., Kasting, J., and Lammer, H. (2007) M stars as targets for terrestrial exoplanet searches and biosignature detection. *Astrobiology* 7:85–166.

Seager, S., Kuchner, M., Hier-Majumder, C.A., and Militzer, B. (2007) Mass-radius relationships for solid exoplanets. *Astrophys J* 669:1279–1297.

Seager, S., Deming, D., and Valenti, J.A. (2009) Transiting exoplanets with JWST. In *Astrophysics in the Next Decade: The James Webb Space Telescope and Concurrent Facilities,* edited by H.A. Thronson, M. Stiavelli, and A. Tielens, Springer, New York, pp 123–145.

Segatz, M., Spohn, T., Ross, M.N., and Schubert, G. (1988) Tidal dissipation, surface heat flow, and figure of viscoelastic models of Io. *Icarus* 75:187–206.

Segura, A., Walkowicz, L.M., Meadows, V., Kasting, J., and Hawley, S. (2010) The effect of a strong stellar flare on the atmospheric chemistry of an Earth-like planet orbiting an M dwarf. *Astrobiology* 10:751–771.

Selsis, F., Kasting, J.F., Levrard, B., Paillet, J., Ribas, I., and Delfosse, X. (2007) Habitable planets around the star Gliese 581? *Astron Astrophys* 476:1373–1387.

Showman, A.P. and Polvani, L.M. (2011) Equatorial superrotation on tidally locked exoplanets. *Astrophys J* 738, doi:10.1088/0004-637X/738/1/71.

Simpson, G.C. (1927) Some studies on terrestrial radiation. *Memoirs of the Royal Meteorological Society* 11:69–95.

Sotin, C., Grasset, O., and Mocquet, A. (2007) Mass–radius curve for extrasolar Earth-like planets and ocean planets. *Icarus* 191:337–351.

Spencer, J.R., Rathbun, J.A., Travis, L.D., Tamppari, L.K., Barnard, L., Martin, T.Z., and McEwen, A.S. (2000) Io's thermal emission from the Galileo photopolarimeter-radiometer. *Science* 288:1198–1201.

Stevenson, D.J. (2010) Planetary magnetic fields: achievements and prospects. *Space Sci Rev* 152:651–664.

Strom, R.G., Terrile, R.J., Hansen, C., and Masursky, H. (1979) Volcanic eruption plumes on Io. *Nature* 280:733–736.

Swift, D.C., Eggert, J.H., Hicks, D.G., Hamel, S., Caspersen, K., Schwegler, E., Collins, G.W., Nettelmann, N., and Ackland, G.J. (2012) Mass-radius relationships for exoplanets. *Astrophys J* 744, doi:10.1088/0004-637X/744/1/59.

Tamuz, O., Ségransan, D., Udry, S., Mayor, M., Eggenberger, A., Naef, D., Pepe, F., Queloz, D., Santos, N.C., Demory, B.-O., Figuera, P., Marmier, M., and Montagnier, G. (2008) The CORALIE survey for southern extra-solar planets. XV. Discovery of two eccentric planets orbiting HD 4113 and HD 156846. *Astron Astrophys* 480:L33–L36.

Tarter, J.C., Backus, P.R., Mancinelli, R.L., Aurnou, J.M., Backman, D.E., Basri, G.S., Boss, A.P., Clarke, A., Deming, D., Doyle, L.R., Feigelson, E.D., Freund, F., Grinspoon, D.H., Haberle, R.M., Hauck, S.A., II, Heath, M.J., Henry, T.J., Hollingsworth, J.L., Joshi, M.M., Kilston, S., Liu, M.C., Meikle, E., Reid, I.N., Rothschild, L.J., Scalo, J., Segura, A., Tang, C.M., Tiedje, J.M., Turnbull, M.C., Walkowicz, L.M., Weber, A.L., and Young, R.E. (2007) A reappraisal of the habitability of planets around M dwarf stars. *Astrobiology* 7:30–65.

Tian, F. (2009) Thermal escape from super Earth atmospheres in the habitable zones of M stars. *Astrophys J* 703:905–909.

Touma, J. and Wisdom, J. (1994) Evolution of the Earth-Moon system. *Astron J* 108:1943–1961.

Tsiganis, K., Gomes, R., Morbidelli, A., and Levison, H.F. (2005) Origin of the orbital architecture of the giant planets of the Solar System. *Nature* 435:459–461.

Turcotte, D.L. (1996) Magellan and comparative planetology. *J Geophys Res* 101:4765–4773.

Tyler, R. (2011) Tidal dynamical considerations constrain the state of an ocean on Enceladus. *Icarus* 211:770–779.

Tyler, R.H. (2008) Strong ocean tidal flow and heating on moons of the outer planets. *Nature* 456:770–772.

Udry, S., Bonfils, X., Delfosse, X., Forveille, T., Mayor, M., Perrier, C., Bouchy, F., Lovis, C., Pepe, F., Queloz, D., and Bertaux, J.-L. (2007) The HARPS search for southern extra-solar planets. XI. Super-Earths (5 and 8 $M_{\oplus}$) in a 3-planet system. *Astron Astrophys* 469:L43–L47.

Valencia, D., Sasselov, D.D., and O'Connell, R.J. (2007) Detailed models of super-Earths: how well can we infer bulk properties? *Astrophys J* 665:1413–1420.

Valencia, D., Ikoma, M., Guillot, T., and Nettelmann, N. (2010) Composition and fate of short-period super-Earths. The case of CoRoT-7b. *Astron Astrophys* 516:A20.

Veeder, G.J., Matson, D.L., Johnson, T.V., Blaney, D.L., and Goguen, J.D. (1994) Io's heat flow from infrared radiometry: 1983–1993. *J Geophys Res* 99:17095–17162.

Vogt, S.S., Butler, R.P., Rivera, E.J., Haghighipour, N., Henry, G.W., and Williamson, M.H. (2010) The Lick-Carnegie exoplanet survey: a 3.1 $M_{\oplus}$ planet in the habitable zone of the nearby M3V star Gliese 581. *Astrophys J* 723:954–965.

von Bloh, W., Bounama, C., Cuntz, M., and Franck, S. (2007) The habitability of super-Earths in Gliese 581. *Astron Astrophys* 476:1365–1371.

Watson, A.J., Donahue, T.M., and Walker, J.C.G. (1981) The dynamics of a rapidly escaping atmosphere: applications to the evolution of Earth and Venus. *Icarus* 48:150–166.

Watson, A.J., Donahue, T.M., and Kuhn, W.R. (1984) Temperatures in a runaway greenhouse on the evolving Venus: implications for water loss. *Earth Planet Sci Lett* 68:1–6.

Weidenschilling, S.J. and Marzari, F. (1996) Gravitational scattering as a possible origin for giant planets at small stellar distances. *Nature* 384:619–621.

Weinberg, N.N., Arras, P., Quataert, E., and Burkart, J. (2011) Nonlinear tides in close binary systems. arXiv:1107.0946.

West, A.A., Hawley, S.L., Bochanski, J.J., Covey, K.R., Reid, I.N., Dhital, S., Hilton, E.J., and Masuda, M. (2008) Constraining

the age-activity relation for cool stars: the Sloan Digital Sky Survey Data Release 5 low-mass star spectroscopic sample. *Astron J* 135:785–795.

Wetherill, G.W. and Stewart, G.R. (1989) Accumulation of a swarm of small planetesimals. *Icarus* 77:330–357.

Williams, D.M. and Pollard, D. (2002) Earth-like worlds on eccentric orbits: excursions beyond the habitable zone. *International Journal of Astrobiology* 1:61–69.

Winn, J.N., Matthews, J.M., Dawson, R.I., Fabrycky, D., Holman, M.J., Kallinger, T., Kuschnig, R., Sasselov, D., Dragomir, D., Guenther, D.B., Moffat, A.F.J., Rowe, J.F., Rucinski, S., and Weiss, W.W. (2011) A super-Earth transiting a naked-eye star. *Astrophys J* 737:L18.

Wisdom, J. (2008) Tidal dissipation at arbitrary eccentricity and obliquity. *Icarus* 193:637–640.

Wordsworth, R.D., Forget, F., Selsis, F., Millour, E., Charnay, B., and Madeleine, J.-B. (2011) Gliese 581d is the first discovered terrestrial-mass exoplanet in the habitable zone. *Astrophys J* 733:L48.

Yelle, R.V. (2004) Aeronomy of extra-solar giant planets at small orbital distances. *Icarus* 170:167–179.

Yoder, C.F. (1995) Astrometric and geodetic properties of Earth and the Solar System. In *Global Earth Physics: A Handbook of Physical Constants,* edited by T.J. Ahrens, American Geophysical Union, Washington, DC, pp 1–31.

Zahn, J.-P. (1977) Tidal friction in close binary stars. *Astron Astrophys* 57:383–394.

Zahn, J.-P. and Bouchet, L. (1989) Tidal evolution of close binary stars. II—Orbital circularization of late-type binaries. *Astron Astrophys* 223:112–118.

Zechmeister, M., Kürster, M., and Endl, M. (2009) The M dwarf planet search programme at the ESO VLT+UVES. A search for terrestrial planets in the habitable zone of M dwarfs. *Astron Astrophys* 505:859–871.

Address correspondence to:
Rory Barnes
Department of Astronomy
University of Washington
Box 351580
Seattle, WA 98195

E-mail: rory@astro.washington.edu

Submitted 15 March 2012
Accepted 28 November 2012